Table 2. Relationship between TM9SF3 expression and clinicopathological parameters in 91 GC cases, evaluated by immunohistochemistry

	TM9SF3 expression		*P* value
	Positive	Negative	
Age			
≤65 years (n = 49)	26 (53%)	23	NS
>65 years (n = 42)	20 (48%)	22	
Gender			
Male (n = 51)	21 (41%)	30	NS
Female (n = 40)	25 (63%)	15	
T grade			
T1 (n = 28)	8 (29%)	20	0.0065
T2/T3/T4 (n = 63)	38 (60%)	25	
N grade			
N0 (n = 25)	7 (28%)	18	0.0101
N1/N2/N3 (n = 66)	39 (59%)	27	
M grade			
M0 (n = 76)	37 (49%)	39	NS
M1 (n = 15)	9 (60%)	6	
Stage			
Stage I (n = 28)	8 (29%)	20	0.0065
Stage II/III/IV (n = 63)	38 (60%)	25	
Histology			
Differentiated (n = 45)	17 (38%)	28	0.0213
Undifferentiated (n = 46)	29 (63%)	17	
Scirrhous (n = 27)	18 (67%)	9	0.0156
Non-scirrhous (n = 19)	5 (26%)	14	

P values were calculated by Fisher's exact test. Histology was determined according to Japanese Classification of Gastric Carcinomas. NS = Not significant.

prognosis in highly expressed GC cases, suggesting that TM9SF3 may be associated with cancer cell growth and invasion ability. However, the biological signifcance of TM9SF3 in GC has not been studied. Initially, we investigated TM9SF3 expression on 9 GC cell lines (Fig. 4a) and found strong expression in HSC-39 and MKN-28 cell lines. HSC-39 is derived from signet ring cell carcinoma of the stomach and is an ideal cell line for this study. Unfortunately, it is a floating cancer cell line and difficult to transfect and process for experimental procedures, and so we utilized MKN-28 cells for the following analyses. Gene silencing in MKN-28 cells were confirmed by Western blot (Fig. 4b). To investigate the possible proliferative effect of TM9SF3, we performed an MTT assay 2 days after TM9SF3-siRNAs and negative control siRNA transfection. There was no significant difference between TM9SF3 siRNA-transfected MKN-28 cells and negative control siRNA-transfected cells (Fig. 4c). Next, to determine the possible role of TM9SF3 in the invasiveness of GC cells, a transwell invasion assay was performed in the MKN-28 GC cell line. Invasion ability was significantly downregulated in

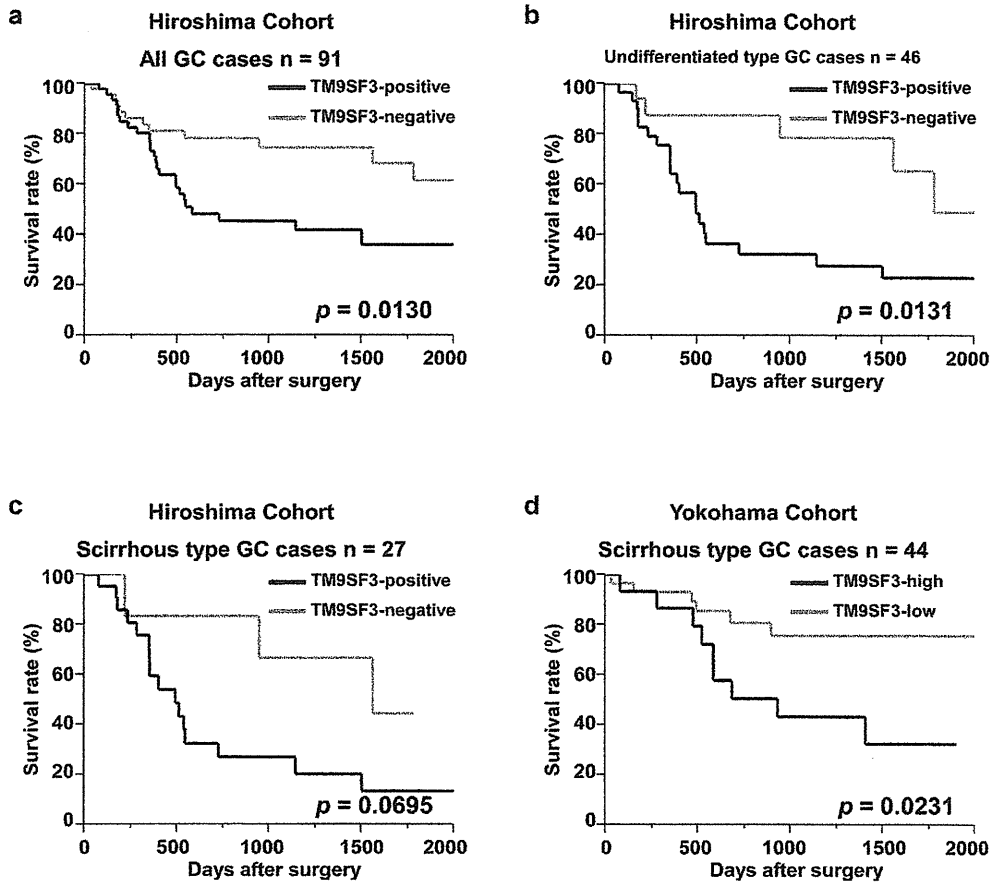

Fig. 3. Cancer specific survival in two separate cohorts; Hiroshima cohort (n = 91, immunostaining) and Yokohama cohort (n = 227, qRT-PCR). *P* value (log-rank test) is shown in the right lower quadrant of each panel. **(a)** Patient prognosis of positive TM9SF3 expression in all GC cases, using immunohistological data. **(b)** Analysis of undifferentiated type GC cases. **(c and d)** Kaplan-Meier plots of the cancer-specific mortality of scirrhous type GC cases in the Hiroshima and Yokohama cohorts, respectively.

TM9SF3 knockdown GC cells compared with negative control siRNA-transfected GC cells (Fig. 4d). These data verify that TM9SF3 is associated with invasion of cancer cells, but not with cancer cell growth in vitro.

Discussion

In the present study, we generated CAST libraries from 2 scirrhous type GC tissues, and identified several genes that encode transmembrane proteins present in scirrhous type GC. This is the first article analyzing surgically resected GC tissue samples by CAST method. We emphasized on transmembrane proteins for their central role as putative novel biomarkers and therapeutic targets and observed that TM9SF3 showed the highest clone count in the candidate list of the scirrhous CAST library. Both quantitative RT-PCR analysis and immunohistochemistry revealed that TM9SF3 was frequently overexpressed in GC. The distribution of TM9SF3 in metastatic lymph nodes also showed the high concordance rate. With regard to the TM9SF3 upregulation, this could be explained by gain of DNA copy numbers in chromosome 10q24, which was reported in gastric cancer [31],

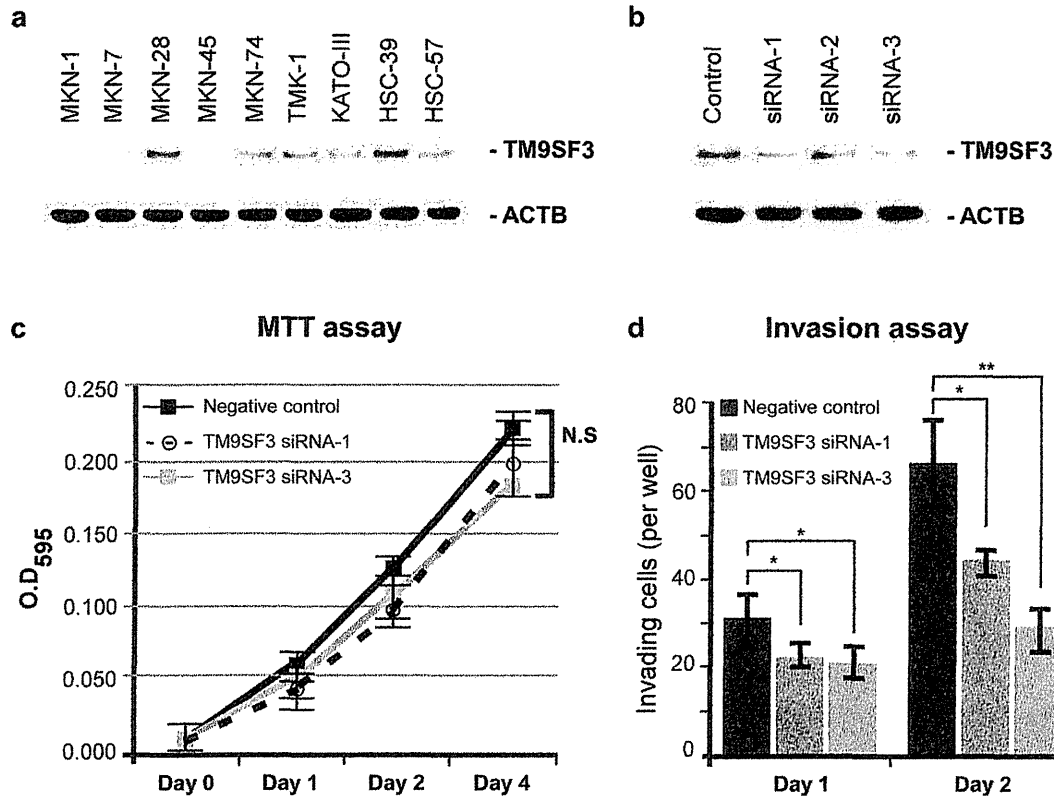

Fig. 4. Effect of TM9SF3 downregulation on cell growth and cell invasion. **(a)** The anti-TM9SF3 antibody detected at ~46 kD band on western blot of nine GC cell lines. β-actin was used as a loading control. **(b)** Western blot analysis of TM9SF3 in MKN-28 GC cells transfected with negative control siRNA or TM9SF3 siRNAs (siRNA 1–3). **(c)** Cell growth was assessed by an MTT assay on 96-well plates in MKN-28 cells. Bars and error bars show mean and s.d. of three different experiments. **(d)** Effect of TM9SF3 knockdown on cell invasion in MKN-28 cells. MKN-28 GC cells transfected with negative control siRNA or TM9SF3 siRNA-1 and siRNA-3 were incubated in Boyden chambers. After 24 and 48-hour incubation, invading cells were counted. Bars and error bars show mean and s.d., respectively of three different experiments. O.D., optical density. N.S., not significant. (*, $P < 0.05$; **, $P < 0.008$).

[32], where TM9SF3 gene is located. In addition, we observed a significant correlation between TM9SF3 expression and poor survival prognosis, in two validation studies.

TM9SF3 encodes transmembrane 9 superfamily member 3 which is one of the members of the TM9SF family. TM9SF members are characterized by a large non-cytoplasmic domain and nine putative transmembrane domains [16]. This family is highly conserved through evolution and four members are reported in mammals (TM9SF1–TM9SF4), suggesting an important biological role for these proteins. However, except for the recently characterized genetic studies in *Dictyostelium* and *Drosophila* showing that TM9SF members are required for adhesion and phagocytosis in innate immune response [33], the biological functions of TM9SF proteins remain largely unknown. Recent studies have demonstrated that human TM9SF1 plays a role in the regulation of autophagy [34] and human TM9SF4 involving in tumor cannibalism and aggressive phenotype of metastatic melanoma cells [35]. Using rat and Chinese Hamster models, Sugasawa et al. [36] have reported that TM9SF3, also known as SMBP, was the first member of TM9SF with functional ligand binding properties. In addition, TM9SF proteins have been found as endosomal or Golgi-like distribution [16] and one of the TM9SF family member, TM9SF2 has been found to be localized in endosomal or lysosomal compartment [37]. It is consistent with our result that TM9SF3 showed cytoplasmic accumulation as well as membranous staining pattern.

Based on our results, TM9SF3 expression was significantly correlated with tumor progression. In scirrhous type GC, MMP-2 produced from stromal fibroblasts is activated by MT1-MMP expressed by GC cells and affects cancer progression in a paracrine manner [38]. Also, fibroblast growth factor-7 (FGF-7) from gastric fibroblasts also affected the growth of scirrhous GC cells [39]. Reciprocally, most fibroblasts were partially regulated by cancer cell-derived growth factors [40] such as, TGFβ, platelet-derived growth factor (PDGF) and FGF2, all of which are key mediators of fibroblast activation and tissue fibrosis [41]. Thus, the growth-promoting factors from GC cells and tumor-specific fibroblasts mutually augment each other's proliferation. Likewise, our present data also demonstrated that TM9SF3 positive scirrhous type GC cases had worse prognosis than negative cases, in both sets of separate cohorts. Here, we suggest that TM9SF3 could establish robust malignant behavior of scirrhous GC cells by acting like a receptor, channel or small molecule transporter in these cancer-stromal cell interactions although the precise function of TM9SF3 is unclear yet. Further investigations are indeed needed to illuminate these hypotheses. On the other hand, in Yokohama cohort, investigated on mRNA level, there was no statistically significant correlation with clinicopathologic parameters including TNM grade and tumor stage. It reflects that mRNA level, actually depends on the amount of tissue obtained and it was difficult to acquire tissue from deeper part of all GC samples.

During in vitro biochemical analyses of TM9SF3, a basement membrane-coated cell invasion assay showed that transient knockdown of TM9SF3 resulted in suppression of invasive capacity of GC cells. We speculate that human TM9SF3 might be involved in an invasive mechanism of GC cells. The next crucial step will be to elucidate how TM9SF3 is involved in the tumor invasion process and whether it is scirrhous type GC specific, in which cancer-stromal interactions have been especially evident. In general, tumor cells at the invasion front are considered to have more aggressive and malignant behavior. Recent study on invasion front of GCs showed that molecular expression of MMP-7, laminin-gamma2 and EGFR was associated with T grade, N grade and tumor stage [42]. However, GC is well known for its intra-tumoral heterogeneity and so, it is difficult to target the whole tumor mass because of such heterogeneous expression of tumor markers. Targeted therapy towards all malignant tumor cells is quite difficult and still required to identify. Here, TM9SF3 stained at both mucosal region and invasion front of tumor mass and thus, it might be a useful therapeutic target for GC.

Taken together, TM9SF3 is a promising prognostic marker for cancer diagnosis of the stomach, especially in scirrhous type GC. Evaluating the molecular mechanism of TM9SF3 involvement in tumor-stroma interactions might improve our understanding of GC carcinogenesis and tumor progression. TM9SF3 expression may be a key factor mediating the biological behavior of the scirrhous type GC. Furthermore, using CAST method, we could identify unknown target genes and novel biomarkers for cancer diagnosis and management. In subsequent study, it might be interesting to examine on a large number of GC samples to study the chemotherapy resistance GC and novel candidates involving towards its molecular mechanism.

Acknowledgments

We thank Mr. Shinichi Norimura for his excellent technical assistance and advice. This work was carried out with the kind cooperation of the Research Center for Molecular Medicine, Faculty of Medicine, Hiroshima University (Hiroshima, Japan). We thank the Analysis Center of Life Science, Hiroshima University, for the use of their facilities. This work was supported in part by Grants-in-Aid for Cancer Research from the Ministry of Education, Culture, Science, Sports, and Technology of Japan, in part by a Grant-in-Aid for the Third Comprehensive 10-Year Strategy for Cancer Control and for Cancer Research from the Ministry of Health, Labor and Welfare of Japan, and in part by the National Cancer Center Research and Development Fund (23-A-9).

Disclosure Statement

The authors have no conflict of interest to disclose.

References

1 Yasui W, Oue N, Kitadai Y, Nakayama H: Recent advances in molecular pathobiology of gastric carcinoma. The Diversity of Gastric Carcinoma: Pathogenesis, Diagnosis and Therapy. Springer Tokyo, Japan 2005;51-71.

2 Lauren P: The two histologcal main types of gastric carcinoma: diffuse and so-called intestinal-type carcinoma. An attempt at histo-clinical classification. Acta Pathol Microbiol Scand 1965;64:31-49.

3 Nakamura K, Sugano H, Takagi K: Carcinoma of the stomach in incipient phase: its histogenesis and histological appearances. Gann 1968;59:251-258.

4 Liu Y, Yoshimura K, Yamaguchi N, Shinmura K, Yokota J, Katai H: Causation of Borrmann type 4 gastric cancer: heritable factors or environmental factors? Gastric Cancer 2003;6:17-23.
5 Yanagihara K, Takigahira M, Tanaka H, Komatsu T, Fukumoto H, Koizumi F, Ochiya T, Ino Y, Hirohashi S: Development and biological analysis of peritoneal metastasis mouse models for human scirrhous stomach cancer. Cancer Sci 2005;96: 323-332.
6 Lockhart DJ, Dong H, Byrne MC, Follettie MT, Gallo MV, Chee MS, Mittmann M, Wang C, Kobayashi M, Horton H, Brown EL: Expression monitoring by hybridization to high-density oligonucleotide arrays. Nat Biotechnol 1996;14:1675-1680.
7 Velculescu VE, Zhang L, Vogelstein B, Kinzler KW: Serial analysis of gene expression. Science 1995;270:484-487.
8 Oue N, Hamai Y, Mitani Y, Matsumura S, Oshimo Y, Aung PP, Kuraoka K, Nakayama H, Yasui W: Gene expression profile of gastric carcinoma: identification of genes and tags potentially involved in invasion, metastasis, and carcinogenesis by serial analysis of gene expression. Cancer Res 2004;64:2397-2405.
9 Oue N, Mitani Y, Aung PP, Sakakura C, Takeshima Y, Kaneko M, Noguchi T, Nakayama H, Yasui W: Expression and localization of Reg IV in human neoplastic and non-neoplastic tissues: Reg IV expression is associated with intestinal and neuroendocrine differentiation in gastric adenocarcinoma. J Pathol 2005;207:185-198.
10 Sentani K, Oue N,Tashiro T, Sakamoto N, Nishisaka T, Fukuhara T, Taniyama K, Matsuura H, Arihiro K, Ochiai A, Yasui W: Immunohistochemical staining of RegIV and claudin-18 is useful in the diagnosis of gastrointestinal signet ring cell carcinoma. Am J Surg Pathol 2008;32: 1182-1189.
11 Oue N, Sentani K, Noguchi T, Ohara S, Sakamoto N, Hayashi T, Anami K, Motoshita J, Ito M, Tanaka S, Yoshida K, Yasui W: Serum olfactomedin 4 (GW112, hGC-1) in combination with Reg IV is a highly sensitive biomarker for gastric cancer patients. Int J Cancer 2009;125:2383-2392.
12 Sentani K, Oue N, Sakamoto N, Arihiro K, Aoyagi K, Sasaki H, Yasui W: Gene expression profiling with microarray and SAGE identifies PLUNC as a marker for hepatoid adenocarcinoma of the stomach. Mod Pathol 2008;21:464-475.
13 Sentani K, Oue N, Sakamoto N, Anami K, Naito Y, Aoyagi K, Sasaki H, Yasui W: Upregulation of connexin 30 in intestinal phenotype gastric cancer and its reduction during tumor progression. Pathobiology 2010;77:241-248.
14 Moon JH, Fujiwara Y, Nakamura Y, Okada K, Hanada H, Sakakura C, Takiguchi S, Nakajima K, Miyata H, Yamasaki M, Kurokawa Y, Mori M, Doki Y: REGIV as a potential biomarker for peritoneal dissemination in gastric adenocarcinoma. J Surg Oncol 2012;105:189-194.
15 Anami K, Oue N, Noguchi T, Sakamoto N, Sentani K, Hayashi T, Hinoi T, Okajima M, Graff JM, Yasui W: Search for transmembrane protein in gastric cancer by the Escherichia coli ampicillin secretion trap: expression of DSC2 in gastric cancer with intestinal phenotype. J Pathol 2010;221:275-284.
16 Pruvot B, Laurens V, Salvadori F, Solary E, Pichon L, Chluba J: Comparative analysis of nonaspanin protein sequences and expression studies in zebrafish. Immunogenetics 2010;62:681-699.
17 Chang H, Jeung HC, Jung JJ, Kim TS, Rha SY, Chung HC: Identification of genes associated with chemosensitivity to SAHA/taxane combination treatment in taxane-resistant breast cancer cells. Breast Cancer Res Treat 2011;125:55-63.
18 Ferguson DA, Muenster MR, Zang Q, Spencer JA, Schageman JJ, Lian Y, Garner HR, Gaynor RB, Huff JW, Pertsemlidis A, Ashfaq R, Schorge J, Becerra C, Williams NS, Graff JM: Selective identification of secreted and transmembrane breast cancer markers using Escherichia coli ampicillin secretion trap. Cancer Res 2005;65:8209-8217.
19 Kadonaga JT, Gautier AE, Straus DR, Charles AD, Edge MD, Knowles JR: The role of the beta-lactamase signal sequence in the secretion of proteins by Escherichia coli. J Biol Chem 1984;259:2149-2154.
20 Japanese classification of gastric carcinoma: 3rd English edition: Gastric Cancer 2011;14:101-112.
21 Kondo T, Oue N, Yoshida K, Mitani Y, Naka K, Nakayama H, Yasui W: Expression of POT1 is associated with tumor stage and telomere length in gastric carcinoma. Cancer Res 2004;64:523-529.
22 Yasui W, Ayhan A, Kitadai Y, Nishimura K, Yokozaki H, Ito H, Tahara E: Increased expression of p34cdc2 and its kinase activity in human gastric and colonic carcinomas. Int J Cancer 1993;53:36-41.
23 Ochiai A, Yasui W, Tahara E: Growth-promoting effect of gastrin on human gastric carcinoma cell line TMK-1. Jpn J Cancer Res 1985;76:1064-1071.
24 Motoyama T, Hojo H, Watanabe H: Comparison of seven cell lines derived from human gastric carcinomas. Acta Pathol Jpn 1986;36:65-83.
25 Sekiguchi M, Sakakibara K, Fujii G: Establishment of cultured cell lines derived from a human gastric carcinoma. Jpn J Exp Med 1978;48:61-68.
26 Yanagihara K, Seyama T, Tsumuraya M, Kamada N, Yokoro K: Establishment and characterization of human signet ring cell gastric carcinoma cell lines with amplification of the c-myc oncogene. Cancer Res 1991;51:381-386.
27 Alley MC, Scudiero DA, Monks A, Hursey ML, Czerwinski MJ, Fine DL, Abbott BJ, Mayo JG, Shoemaker RH, Boyd MR: Feasibility of drug screening with panels of human tumor cell lines using a microculture tetrazolium assay. Cancer Res 1988;48: 589-601.
28 Verjans E, Noetzel E, Bektas N, Schutz AK, Lue H, Lennartz B, Hartmann A, Dahl E, Bernhagen J: Dual role of macrophage migration inhibitory factor (MIF) in human breast cancer. BMC Cancer 2009; 9:230.
29 Holness CL, Simmons DL: Molecular cloning of CD68, a human macrophage marker related to lysosomal glycoproteins. Blood 1993;81:1607-1613.
30 Hack AA, Groh ME, McNally EM: Sarcoglycans in muscular dystrophy. Microsc Res Tech 2000;48:167-180.
31 Noguchi T, Wirtz HC, Michaelis S, Gabbert HE, Mueller W: Chromosomal imbalances in gastric cancer. Correlation with histologic subtypes and tumor progression. Am J Clin Pathol 2001;115:828-834.
32 Saitoh T, Katoh M: FRAT1 and FRAT2, clustered in human chromosome 10q24.1 region, are up-regulated in gastric cancer. Int J Oncol 2001;19:311-315.
33 Cornillon S, Pech E, Benghezal M, Ravanel K, Gaynor E, Letourneur F, Brückert F, Cosson P: Phg1p is a nine- transmembrane protein superfamily member involved in dictyostelium adhesion and phagocytosis. J Biol Chem 2000;275:34287-34292.
34 He P, Peng Z, Luo Y, Wang L, Yu P, Deng W, An Y, Shi T, Ma D: High-throughput functional screening for autophagy-related genes and identification of TM-9F1 as an autophagosome-inducing gene. Autophagy 2009;5:52-60.
35 Lozupone F, Perdicchio M, Brambilla D, Borghi M, Meschini S, Barca S, Marino ML, Logozzi M, Federici C, Iessi E, de Milito A, Fais S: The human homologue of Dictyostelium discoideum phg1A is expressed by human metastatic melanoma cells. EMBO Rep 2009;10:1348-1354.

36 Sugasawa T, Lenzen G, Simon S, Hidaka J, Cahen A, Guillaume JL, Camoin L, Strosberg AD, Nahmias C: The iodocyanopindolol and SM-11044 binding protein belongs to the TM9SF multispanning membrane protein superfamily. Gene 2001;273:227-237.
37 Schimmoller F, Diaz E, Muhlbauer B, Pfeffer SR: Characterization of a 76 kDa endosomal, multispanning membrane protein that is highly conserved throughout evolution. Gene 1998;216:311-318.
38 Yashiro M, Chung YS, Sowa M: Tranilast (N-(3,4-dimethoxycinnamoyl) anthranilic acid) down-regulates the growth of scirrhous gastric cancer. Anticancer Res 1997; 17:895-900.
39 Nakazawa K, Yashiro M, Hirakawa K: Keratinocyte growth factor produced by gastric fibroblasts specifically stimulates proliferation of cancer cells from scirrhous gastric carcinoma. Cancer Res 2003;63: 8848-8852.
40 Tahara E: Abnormal growth factor/ cytokine network in gastric cancer. Cancer Microenviron 2008;1:85-91.
41 Elenbaas B, Weinberg RA: Heterotypic signaling between epithelial tumor cells and fibroblasts in carcinoma formation. Exp Cell Res 2001;264:169-184.
42 Sentani K, Matsuda M, Oue N, Uraoka N, Naito Y, Sakamoto N, Yasui W: Clinicopathological significance of MMP-7, laminin gamma2 and EGFR expression at the invasive front of gastric carcinoma. Gastric Cancer
DOI: 10.1007/s10120-013-0302-6

Supplementary information

Additional supplementary information can be found in online version of this article.

NEOPLASIA
www.neoplasia.com

Volume 15 Number 12 December 2013 pp. 1391–1399 **1391**

Combining Molecular Targeted Drugs to Inhibit Both Cancer Cells and Activated Stromal Cells in Gastric Cancer[1]

[illegible]

Department of Gastroenterology and Metabolism, Graduate School of Biomedical and Health Sciences, Hiroshima University, Hiroshima, Japan; Department of Endoscopy, Hiroshima University Hospital, Hiroshima, Japan; Department of Molecular Pathology, Graduate School of Biomedical and Health Sciences, Hiroshima University, Hiroshima, Japan

Abstract

Recent studies have revealed that PDGF plays a role in promoting progressive tumor growth in several cancers, including gastric cancer. Cancer-associated fibroblasts, pericytes, and lymphatic endothelial cells in stroma express high levels of PDGF receptor (PDGF-R); cancer cells and vascular endothelial cells do not. Mammalian target of rapamycin (mTOR) is a serine/threonine kinase that increases the production of proteins that stimulate key cellular processes such as cell growth and proliferation, cell metabolism, and angiogenesis. In the present study, we examined the effects of PDGF-R tyrosine kinase inhibitor (nilotinib) and mTOR inhibitor (everolimus) on tumor stroma in an orthotopic nude mice model of human gastric cancer. Expression of PDGF-B and PDGF-Rβ mRNAs was associated with stromal volume. Treatment with nilotinib did not suppress tumor growth but significantly decreased stromal reactivity, lymphatic invasion, lymphatic vessel area, and pericyte coverage of tumor microvessels. In contrast, treatment with everolimus decreased tumor growth and microvessel density but not stromal reactivity. Nilotinib and everolimus in combination reduced both the growth rate and stromal reaction. Target molecule-based inhibition of cancer-stromal cell interaction appears promising as an effective antitumor therapy.

Neoplasia (2013) 15, 1391–1399

Introduction

In 2011, gastric cancer was reported as the world's fourth most common cancer in men and fifth most common in women [1]. The major cause of gastric cancer-associated mortality is metastasis. Recent studies in molecular and cellular biology have shown that tumor growth and metastasis are not determined by cancer cells alone but also by various stromal cells. The stroma constitutes a large part of most solid tumors, and the cancer-stromal cell interaction contributes functionally to tumor growth and metastasis [2,3]. Tumor stroma contains many different types of cells, including activated fibroblasts (myofibroblasts), endothelial cells, pericytes, and inflammatory cells. It has become clear that activated fibroblasts in cancer stroma are key modulators of tumor progression. As such, they are called cancer-associated fibroblasts (CAFs) [4]. Although the mechanisms that regulate activation of fibroblasts and their accumulation in tumors are not fully understood, PDGF, transforming growth factor β, and fibroblast growth factor 2 are known to be partly involved in this process [5].

PDGF and PDGF receptor (PDGF-R) are expressed in many human neoplasms, including prostate [6], lung [7], colon [8], and breast [9,10] neoplasms. We previously reported expression of PDGF-R in CAFs [11], pericytes, and lymphatic endothelial cells in the stroma of gastric cancer [12] but not in cancer cells or vascular

Abbreviations: CAF, cancer-associated fibroblast; mTOR, mammalian target of rapamycin; PDGF-R, PDGF receptor; VEGF, vascular endothelial growth factor

Address all correspondence to: Yasuhiko Kitadai, MD, PhD, Department of Gastroenterology and Metabolism, Graduate School of Biomedical and Health Sciences, Hiroshima University, 1-2-3 Kasumi, Minami-ku, Hiroshima 734-8551, Japan.
E-mail: kitadai@hiroshima-u.ac.jp

[1]This work was supported, in part, by grants-in-aid for Cancer Research from the Ministry of Education, Culture, Science, Sports, and Technology of Japan. The authors have no conflict of interest to report.
Received 20 September 2013; Revised 20 September 2013; Accepted 6 November 2013

DOI 10.1593/neo.131668

endothelial cells. PDGF-R signaling is reported to increase proliferation of tumor cells in an autocrine manner [13] and to stimulate angiogenesis [14], recruit pericytes [13,15], and control interstitial fluid pressure in stroma, influencing transvascular transport of chemotherapeutic agents in a paracrine manner [16]. Imatinib mesylate is a protein-tyrosine kinase inhibitor that was developed initially for its selectivity against breakpoint cluster region-Abelson (BCR-ABL) fusion protein [17]. The following additional tyrosine kinases are inhibited by imatinib: c-KIT, the receptor for KIT ligand (stem cell factor), two structurally similar PDGF-Rs (PDGF-Rα and PDGF-Rβ), and discoidin domain receptors (DDR1 and DDR2) [18,19]. Nilotinib has been established as a drug with potency superior to that of imatinib as an inhibitor of BCR-ABL. Nilotinib also inhibits the tyrosine kinase activity of the PDGF and c-KIT receptors DDR1 and DDR2 with efficacy similar that of imatinib [20,21].

The mammalian target of rapamycin (mTOR), a serine/threonine kinase, integrates multiple signaling pathways, including those that control growth and survival of tumor cells and angiogenesis. Mutations in upstream regulators of the mTOR signaling pathway, including epithelial growth factor receptor [22], phosphatidylinositol-3 kinase (PI3K) [22], and phosphatase and tensin homolog (PTEN) [23], have been frequently observed in human gastric cancer tissues. Phosphorylated mTOR, indicative of mTOR activation [24], has been positively correlated with tumor progression and poor survival in patients with gastric cancer [24,25]. mTOR exists in two complexes, mTORC1 and mTORC2 [26]. mTORC1 activation controls cell growth by regulating translation, ribosome biogenesis, autophagy, and metabolism [27]. mTORC2 phosphorylates Akt, serum/glucocorticoid regulated kinase 1 (SGK1), and protein kinase C to control multiple functions including cell survival and cytoskeletal organization [28]. mTOR also increases the translation of hypoxia-inducible factor 1α, which drives the expression of angiogenic growth factors such as vascular endothelial growth factor (VEGF), resulting in new vasculature. Everolimus is one of the rapalogs that inhibit mTORC1-mediated phosphorylation of S6 kinase 1 (S6K1) and 4E-binding protein 1 (4E-BP1), leading to decreased cell migration and invasion [29].

We examined, in an orthotopic nude mice model, whether nilotinib and everolimus have a synergic inhibitory effect on growth and metastasis of gastric cancer. We focused on cancer-stromal cell interactions because both the molecules and the cells targeted by these two drugs differ.

Materials and Methods

Human Gastric Cancer Cell Lines and Culture Conditions

Three gastric cancer cell lines, including high PDGF-B–expressing cells (TMK-1 and MKN-1) and low PDGF-B–expressing cells (KKLS), were used in this study [12]. The TMK-1 cell line (poorly differentiated adenocarcinoma) was kindly provided by Dr E. Tahara (Hiroshima University, Hiroshima, Japan). The MKN-1 cell line (adenosquamous carcinoma) was obtained from the Health Science Research Resources Bank (Osaka, Japan), and the KKLS cell line (undifferentiated carcinoma) was kindly provided by Dr Y. Takahashi (International University of Health and Welfare, Chiba, Japan). These cell lines were maintained in Dulbecco's Modified Eagle's Medium with 10% FBS (Sigma-Aldrich, St Louis, MO) and a penicillin-streptomycin mixture.

Animals and Orthotopic Implantation of Tumor Cells

Female athymic nude BALB/c mice were obtained from Charles River Japan (Tokyo, Japan). The mice were maintained under specific pathogen-free conditions and used at 5 weeks of age. The study was carried out after permission was granted by the Committee on Animal Experimentation of Hiroshima University. TMK-1, MKN-1, and KKLS cells were harvested from subconfluent cultures by brief exposure to 0.25% trypsin and 0.02% EDTA. Trypsinization was stopped with medium containing 10% FBS, and the cells were washed once in serum-free medium and resuspended in Hank's balanced salt solution. Only suspensions consisting of single cells with >90% viability were used. To produce gastric tumors, 1×10^6 cells in 50 μl of Hank's balanced salt solution were injected into the gastric wall of nude mice under observation with a zoom stereomicroscope (Carl Zeiss, Gottingen, Germany).

Treatment of Established Human Gastric Cancer Tumors Growing in the Gastric Wall of Nude Mice

To compare the therapeutic effects of imatinib and nilotinib on stromal cells, we performed preliminary experiments. The optimal biologic dose was used, as determined previously [30–32]. Seven days after the orthotopic implantation of TMK-1 or MKN-1 tumor cells, mice were randomized into the following three groups: those given water daily by oral gavage (control group), those given 50 mg/kg per day imatinib by oral gavage, and those given 50 mg/kg per day nilotinib by oral gavage. Treatments continued for 21 days, and the mice were killed on day 22. Excised tumors were subjected to immunohistochemistry.

To compare and evaluate the effect of combination therapy, 14 days after orthotopic implantation of TMK-1 tumor cells, mice were randomized to one of the following four treatments ($n = 6$ in each group): 1) daily oral gavage of water (control group), 2) daily oral gavage of nilotinib (100 mg/kg; nilotinib group), 3) daily oral gavage of everolimus (2 mg/kg; everolimus group), and 4) daily oral gavage of nilotinib (100 mg/kg) and everolimus (2 mg/kg; combination group). Combination studies with imatinib and everolimus were not performed due to drug-drug interactions that effect the pharmacokinetic profiles and tolerability of the agents *in vivo*. The mice were treated for 35 days, and then killed and subjected to necropsy.

Necropsy Procedures and Histologic Studies

Mice bearing orthotopic tumors were killed by diethyl ether. Body weights were recorded. After necropsy, tumors were excised and weighed. For immunohistochemistry, one part of the tumor tissue was fixed in formalin-free IHC Zinc Fixative (BD Pharmingen, San Diego, CA) and embedded in paraffin, and the other part was embedded in OCT Compound (Miles Laboratories, Elkhart, IN), rapidly frozen in liquid nitrogen, and stored at −80°C. All macroscopically enlarged regional (celiac and para-aortal) lymph nodes were harvested, and the presence of metastatic disease was confirmed by histologic examination.

Patients and Tumor Specimens

To examine the clinical importance of PDGF/receptor signaling and mTOR signaling, endoscopic biopsy or surgical specimens were obtained from 29 patients with gastric cancer who underwent surgical resection at Hiroshima University Hospital. The specimens were examined by quantitative RT-PCR (RT-PCR) and immunohistochemistry, respectively. The biopsy specimens were snap frozen in

liquid nitrogen and stored at -80°C until RNA extraction. Use of the specimens was in accordance with the Ethical Guidelines for Human Genome/Gene Research of the Japanese Government. Patient informed consent was not required, but identifying information for all samples was removed before analysis.

Quantitative RT-PCR Analysis

Total RNA was extracted from the gastric cancer cell lines and biopsy specimens with an RNeasy Kit (Qiagen, Valencia, CA) according to the manufacturer's instructions. cDNA was synthesized from 1 μg of total RNA with a first-strand cDNA synthesis kit (Amersham Biosciences, Piscataway, NJ). After reverse transcription of RNA into cDNA, quantitative RT-PCR was performed with a LightCycler FastStart DNA Master SYBR Green I kit (Roche Diagnostics, Basel, Switzerland) according to the manufacturer's recommended protocol. Reactions were carried out in triplicate. To correct for differences in both RNA quality and quantity between samples, values were normalized to those of glyceraldehyde-3-phosphate dehydrogenase (GAPDH). The mRNA ratio between gastric carcinoma tissues (T) and corresponding normal mucosa (N) was calculated and expressed as the T/N ratio. Primers for PCR were designed with specific primer analysis software (Primer Designer; Scientific and Educational Software, Cary, NC), and specificity of the sequences was confirmed by FASTA [European Molecular Biology Laboratory (EMBL) Database, Heidelberg, Germany]. Respective primer sequences, annealing temperatures, and PCR cycles were as previously reported [12].

Reagents

Imatinib (Gleevec), nilotinib (Tasigna), and everolimus (Afinitor) were kindly provided by Novartis Pharma (Basel, Switzerland). Imatinib and everolimus were diluted in sterile water for oral administration. Nilotinib was disolved in 0.5% hydroxypropylmethylcellulose aqueous solution containing 0.05% Tween 80 at the concentration of 4 mg/ml and then diluted in sterile water. Primary antibodies were purchased as follows: polyclonal rabbit anti–PDGF-Rβ, polyclonal rabbit antiphosphorylated PDGF-Rβ (p–PDGF-Rβ), and polyclonal rabbit anti-human VEGF-A (sc-152) from Santa Cruz Biotechnology (Santa Cruz, CA); rat anti-mouse CD31 [(platelet endothelial cell adhesion molecule (PECAM1)] from BD Pharmingen; mouse anti-desmin monoclonal antibody from Molecular Probes (Eugene, OR); rabbit anti–α-smooth muscle actin (α-SMA; ab5694) from Abcam (Cambridge, United Kingdom); Ki-67–equivalent antibody (MIB-1) from Dako (Carpinteria, CA); monoclonal rat anti-mouse lymphatic vessel endothelial hyaluronan receptor 1 (Lyve-1) antibody from R&D Systems (Minneapolis, MN); polyclonal rabbit anti-mouse type I collagen from Novotec (Saint Martin La Garenne, France); and monoclonal rabbit anti-mouse S6 ribosomal protein antibody (No. 2217) and monoclonal rabbit antiphosphorylated mouse S6 ribosomal protein antibody (No. 4858) from Cell Signaling Technology (Beverly, MA). The following fluorescent secondary antibodies were used: Alexa 488-conjugated goat anti-rabbit IgG, Alexa 488-conjugated goat anti-rat IgG, and Alexa 546-conjugated goat anti-rabbit IgG (all from Molecular Probes).

Immunofluorescence for PDGF-Rβ and p–PDGF-Rβ and Double Immunofluorescence for CD31 (Vascular Endothelial Cells) and Desmin (Pericytes)

Fresh-frozen specimens of TMK-1 human gastric cancer tissue obtained from nude mice were cut into 8-μm sections and mounted on positively charged slides. After fixation with ice-cold acetone for 20 minutes, washing and blocking were performed as previously described [11]. The slides were incubated for 3 hours at room temperature with primary antibody against PDGF-Rβ or p–PDGF-Rβ. Slides were incubated for 1 hour at room temperature with Alexa 546-conjugated goat anti-rabbit IgG secondary antibody and then nuclear counterstained with 4′,6-diamidino-2-phenylindole (DAPI) for 10 minutes. PDGF-Rβ or p–PDGF-Rβ was identified by red fluorescence.

For double immunofluorescence, after fixation, washing, and blocking, the slides were incubated overnight at 4°C with Fab fragment goat anti-mouse IgG (Jackson ImmunoResearch Laboratories, West Grove, PA) to block endogenous immunoglobulins. Then, slides were incubated with the primary antibody desmin for 3 hours at room temperature. This was followed by incubation for 1 hour at room temperature with Alexa 546-conjugated goat anti-mouse IgG secondary antibody. Slides were then incubated for 3 hours at room temperature with antibody against CD31 and incubated for 1 hour at room temperature with Alexa 488-conjugated goat anti-rat IgG secondary antibody. The samples were then nuclear counterstained with DAPI. Endothelial cells were identified by green fluorescence, whereas pericytes were identified by red fluorescence. The coverage of pericytes on endothelial cells was determined by counting CD31-positive cells in direct contact with desmin-positive cells in five randomly selected microscopic fields (at ×200 magnification) [33].

Confocal Microscopy

Confocal fluorescence images were obtained with the use of a ×20 or ×40 objective lens on a Carl Zeiss LSM laser scanning microscopy system (Carl Zeiss Inc, Thornwood, NY).

Immunohistochemistry and Terminal Deoxynucleotide Transferase-Mediated dUTP-Biotin Nick End Labeling

Immunohistochemistry for α-SMA, type I collagen, Ki-67, Lyve-1, phosphorylated S6 ribosomal protein, or VEGF-A was performed on formalin-free zinc-fixed, paraffin-embedded tissues cut into serial 4-μm sections. After deparaffinization and rehydration, tissue sections to be stained for α-SMA, type I collagen, Ki-67, Lyve-1, phosphorylated S6 ribosomal protein, or VEGF-A were pretreated by microwaving them twice for 5 minutes in Dako REAL Target Retrieval Solution (Dako). Primary antibodies were applied to the slides and incubated overnight in humidified boxes at 4°C. After incubation for 1 hour at room temperature with corresponding peroxidase-conjugated secondary antibodies, a positive reaction was detected by exposure to stable DAB for 5 to 10 minutes. Slides were counterstained with hematoxylin for visualization of the nucleus. Apoptotic cells in tissue sections were detected by terminal deoxynucleotide transferase-mediated deoxyuridine triphosphates (dUTP)-biotin nick end labeling (TUNEL) assay with the ApopTag Plus Peroxidase *In Situ* Apoptosis Detection Kit (Chemicon Intl, Temecula, CA) according to the manufacturer's instructions.

Quantification of the CAF (α-SMA–Positive), Collagen (Type I Collagen-Positive), Microvessel (CD31-Positive), and Lymphatic Vessel (Lyve-1–Positive) Areas

To evaluate angiogenic and lymphangiogenic activity of the tumors, the areas of vascular and lymphatic microvessels were quantified. Ten random fields at ×200 (for vascular microvessels) or ×100 (for lymphatic microvessels) magnification were captured for each tumor, and the outline of each vascular or lymphatic microvessel including a lumen was manually traced. The areas were then calculated with

the use of National Institutes of Health ImageJ software (Wayne Rasband, Bethesda, MD). The areas of CAFs and extracellular matrix (ECM) were also determined from the respective areas of α-SMA–positive and type I collagen-positive staining from 10 optical fields (original magnification, ×100) of different sections.

Determination of the Ki-67 Labeling Index and the Apoptotic Index

The Ki-67 labeling index (Ki-67 LI) was determined by light microscopy at the site of the greatest number of Ki-67–positive cells. Cells were counted in 10 fields at ×200 magnification, and the number

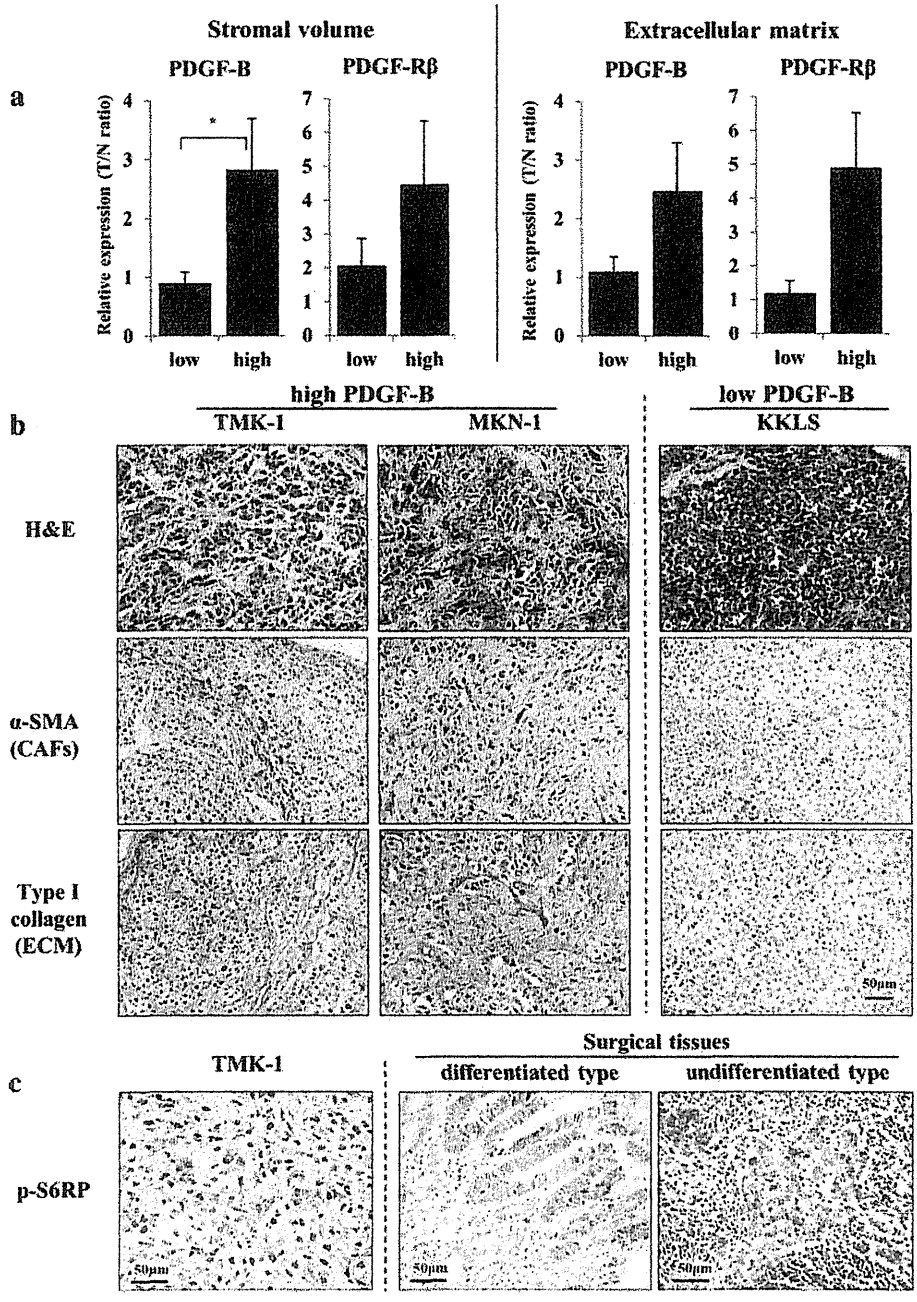

Figure 1. Expression of PDGF-B and PDGF-Rβ mRNAs in relation to stromal volume and ECM production in human gastric cancer tissues (A). Stromal volume and ECM production were evaluated by immunostaining for α-SMA and type I collagen, respectively. Tissues were classified as those with low (below median value) and those with high (higher than median value) expression levels. T/N ratio is the ratio of expression in cancer tissue to that of normal mucosa. The bars represent means + SE. *$P < .05$. Hematoxylin and eosin (H&E) staining and immunohistochemistry for α-SMA and type I collagen in orthotopic xenografts (B). Tumors with high PDGF-B mRNA expression (TMK-1 and MKN-1 tumors) have rich stroma, whereas tumors with low PDGF-B mRNA expression (KKLS tumors) have scanty stroma. CAFs are cancer-associated fibroblasts. Immunohistochemistry for p-S6RPs in primary gastric cancer tissue (C). Expression of p-S6RP is detected in cytoplasm of cancer cells in TMK-1 orthotopic tumor and in differentiated and undifferentiated human gastric cancers.

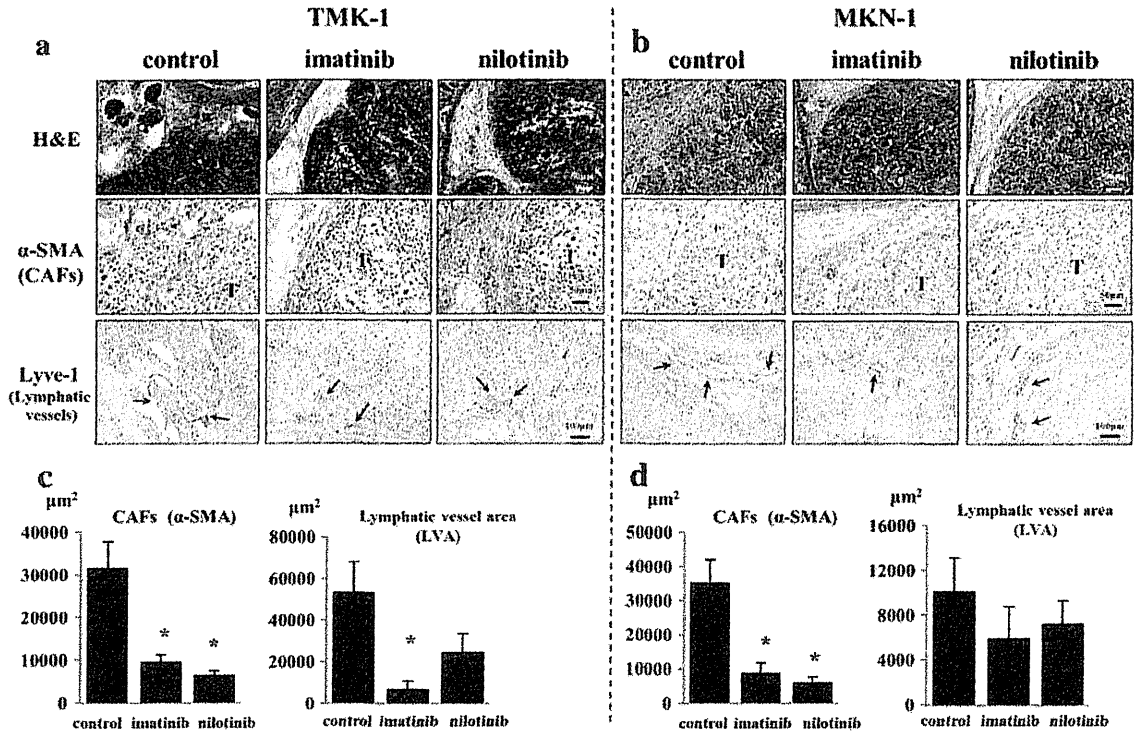

Figure 2. Effects of imatinib and nilotinib on stroma of TMK-1 and MKN-1 tumors. H&E staining and immunohistochemistry for α-SMA and Lyve-1 in TMK-1 (A) and MKN-1 (B) orthotopic tumors are shown. The stromal reaction (evaluated by immunostaining for α-SMA) was significantly reduced in mice treated with imatinib and nilotinib in comparison to that in control group mice (C and D). Lymphatic vessel area (Lyve-1–positive area) decreased especially in the group of mice with TMK-1 tumors treated with imatinib and nilotinib (C and D). T, tumor nest; arrows, dilated lymphatic vessels. *$P < .05$; bars, SE.

of positive cells among approximately 300 tumor cells was counted and expressed as a percentage. The number of apoptotic cells was counted in 10 random 0.14-mm^2 fields at ×200 magnification. The apoptotic index was taken as the ratio of positively stained tumor cells and bodies to all tumor cells and expressed as a percentage for each case.

Statistical Analysis

Values are expressed as means ± SE. Between-group differences in murine body weight, tumor weight, and the areas of α-SMA–positive, type I collagen-positive, CD31-positive, and Lyve-1–positive cells were analyzed by Wilcoxon/Kruskal-Wallis test. Differences in the incidence of lymph node metastasis were analyzed by Fisher's exact test. Differences in the percentages of Ki-67–positive cells and TUNEL-positive cells were analyzed by unpaired Student's t test or χ^2 test as appropriate. A P value of <.05 was considered statistically significant.

Results

Expression of PDGF-B and PDGF-Rβ in Relation to Stromal Reaction in Human Gastric Cancers

We first examined mRNA expression levels of PDGF-B and PDGF-Rβ in relation to stromal reaction in human gastric cancer tissues. Stromal reaction was evaluated as stromal volume and as ECM production by immunohistochemistry for α-SMA and type I collagen, respectively (Figure 1*A*). Stromal volume was significantly higher in the PDGF-B–high group than in the PDGF-B–low group. ECM production tended to be greater in the PDGF-B–high group. PDGF-Rβ expression was clearly related to stromal reaction.

TMK-1 and MKN-1 cells (high PDGF-B–expressing cells) produced orthotopic tumors with abundant stroma; however, KKLS cells (low PDGF-B–expressing cells) did not (Figure 1*B*). Thus, the PDGF/receptor system may be involved in tumor–stromal cell interaction.

Table 1. Effects of Nilotinib and Everolimus on Orthotopic TMK-1 Tumors per Treatment Group.

Group	Body Weight (g)	Tumor Incidence	Tumor Weight (g)	Lymph Node Metastasis
Control	21.8 (17.8-24.6)	5/5	0.33 (0.07-0.72)	3/5
Nilotinib (100 mg/kg)	20.6 (18.5-23.5)	5/5	0.35 (0.10-0.45)	4/5
Everolimus (2 mg/kg)	22.0 (20.4-23.9)	4/6	0.08 (0.00-0.15)*	3/6
Nilotinib (100 mg/kg) + everolimus (2 mg/kg)	21.3 (16.3-22.1)	1/6	0.006 (0.00-0.04)†	0/6

Control group ($n = 5$), nilotinib group ($n = 5$), everolimus group ($n = 6$), and nilotinib plus everlimus group ($n = 6$).
Ranges are shown in parentheses.
*$P < .05$ *versus* control group values.
†$P < .01$ *versus* control group values.

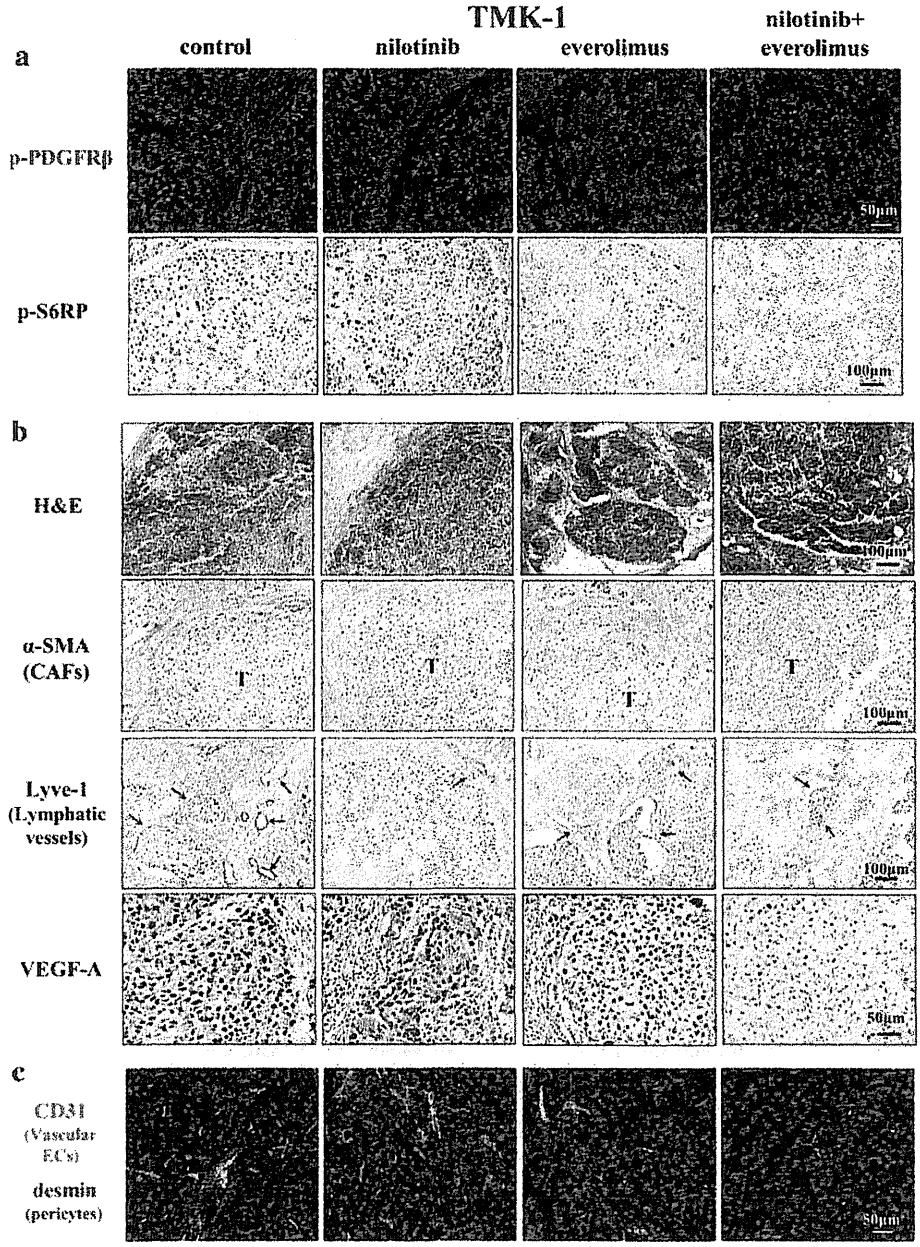

Figure 3. Effects of nilotinib and/or everolimus on TMK-1 orthotopic tumors. Phosphorylation of downstream target protein for nilotinib and everolimus. Treatment with nilotinib inhibited expression of p–PDGF-Rβ. Treatment with everolimus inhibited phosphorylation of S6RP (A). H&E and immunohistochemical staining for α-SMA, Lyve-1, and VEGF-A in TMK-1 orthotopic gastric tumor (B). Effects of nilotinib and everolimus on microvessels in TMK-1 tumor. Pericyte coverage on tumor-associated endothelial cells in the TMK-1 gastric tumors (C). Treatment with nilotinib reduced pericyte coverage of microvessels. Vascular endothelial cells were identified by green fluorescence, whereas desmin (pericytes) were identified by red fluorescence.

Activation of mTOR Signaling Pathway in Human Gastric Cancers

We next examined activation of the mTOR pathway in human gastric cancer tissues obtained surgically. Phosphorylation of S6 (p-S6) ribosomal proteins (p-S6RP) was assessed to evaluate activity of the mTOR signaling pathway. In all 29 human gastric cancers, tumor cells were shown by immunohistochemistry to express p-S6RP. Although expression of p-S6RP was detected in both differentiated and undifferentiated gastric cancers (Figure 1*C*), the staining was heterogeneous; that is, it was weak at the invasive edge (staining not shown). Tumor cells in xenografts implanted into nude mice were also positive for p-S6RP (Figure 1*C*).

Effects of Imatinib and Nilotinib on Tumor Stroma

In the first set of animal experiments, we examined the effects of PDGF-R tyrosine kinase inhibitors, imatinib and nilotinib, on stroma of TMK-1 and MKN-1 tumors. The stromal reaction at the tumor

periphery was significantly reduced in mice treated with imatinib or nilotinib in comparison to that in control mice (Figure 2, *A* and *B*). A decrease in the lymphatic vessel area (Lyve-1–positive area) was also noted, especially in the TMK-1 tumors of mice treated with both imatinib and nilotinib (Figure 2, *A* and *C*).

Combining Treatment of Human Gastric Cancer Growing in the Gastric Wall of Nude Mice

We next determined whether nilotinib and everolimus, administered in combination, have a synergistic effect. The growth and metastasis of TMK-1 human gastric cancer cells implanted in the gastric wall of nude mice were evaluated. The tumor incidence was 100% in all treatment groups. Toxicity of the various treatment regimens was assessed on the basis of change in body weight. Oral administration of nilotinib, everolimus, and of the two drugs in combination did not significantly affect body weight (Table 1). Tumor growth and metastasis were not inhibited in mice treated with nilotinib alone (*vs* control mice); however, tumor growth was significantly inhibited in mice treated with everolimus alone. Furthermore, tumor growth was much more inhibited with the combination treatment. In five of six mice, tumors were not detected macroscopically. Lymph node metastasis was significantly inhibited only in mice treated with nilotinib and everolimus in combination (Table 1).

Histopathologic Analysis of TMK-1 Tumors

To assess whether nilotinib and everolimus inhibit targeted molecules, tumor sections were analyzed immunohistochemically for the expression of p–PDGF-Rβ and p-S6RP. The phosphorylation of PDGF-Rβ was significantly inhibited in orthotopic tumors of mice treated with nilotinib alone or with nilotinib and everolimus in combination (Figure 3*A*). The phosphorylation of S6 ribosomal protein was significantly inhibited in orthotopic tumors of mice treated with everolimus alone or nilotinib and everolimus in combination (Figure 3*A*).

The periphery of TMK-1 gastric tumors was adjacent to abundant stroma, into which tumor cells infiltrated. In contrast, gastric tumors in mice treated with nilotinib alone or with nilotinib and everolimus in combination were surrounded by scanty stroma (Figure 3*B* and Table 2). In addition, treatment with everolimus alone or with nilotinib and everolimus in combination significantly reduced the areas of vascular microvessels (Table 2), although treatment with nilotinib alone or with nilotinib and everolimus in combination significantly reduced the number of lymphatic vessels (Figure 3*B* and Table 2). The number of pericytes covering endothelial cells was also decreased (Figure 3*C* and Table 2).

Proliferation of tumor cells was evaluated by staining for Ki-67. The control group Ki-67 LI (39.6 ± 5.2) was significantly decreased with treatment by combination treatment (13.1 ± 2.3; $P < .01$; Table 2).

According to TUNEL assay, the median number of apoptotic tumor cells in control mice was 6.94 ± 1.26. The number of apoptotic cells in tumors of mice from each of the groups treated with everolimus was significantly increased in comparison to the number in control mice (Table 2).

mTOR Inhibitor Reduced Expression of VEGF-A

Treatment with everolimus or nilotinib and everolimus in combination inhibited the number and area of vascular microvessels. Therefore, we examined expression of angiogenic factor VEGF-A. Immunoreactivity of VEGF-A in tumor cells was markedly suppressed by treatment with everolimus (Figure 3*B*).

Discussion

In the present study, treatment with imatinib or nilotinib (PDGF-R tyrosine kinase inhibitor) significantly reduced the stromal reaction, area of lymphatic vessels, and pericyte coverage, consistent with our previously reported findings [11,12]. However, tumor growth and microvessel density were not inhibited. In contrast, treatment with everolimus (mTOR inhibitor) induced apoptosis of tumor cells and inhibited angiogenesis but did not influence the stromal reaction. More interestingly, nilotinib and everolimus administered in combination dramatically inhibited tumor growth, angiogenesis, stromal reaction, and lymph node metastasis. Primary tumors were not detected in five of six mice, and no lymph node metastasis was found in any of the mice in the combination drug group.

Imatinib and nilotinib are well-known multiple tyrosine kinase inhibitors that inhibit mainly BCR-ABL, c-KIT, DDR1, DDR2, and PDGF-Rs. BCR-ABL and c-KIT are not expressed in gastric cancer cells (data not shown). DDRs have been reported to be activated by different types of collagen and participate in several processes such as cell adhesion, migration, and proliferation [34]. So far, there is no report concerning the role of DDRs in human gastric cancer. We reported previously that PDGF ligands are expressed by gastric cancer cells, whereas PDGF-Rs are expressed mainly by stromal cells [12].

Table 2. Immunohistochemical Analysis of TMK-1 Human Gastric Carcinoma Cells per Treatment Group.

Group	Tumor Cells		Vascular Endothelial Cells			Lymphatic Endothelial Cells
	Ki-67 LI* (%)	TUNEL† (%)	MVC‡ (Per Field)	MVA§ (/× 10^3 μm^2)	Pericyte Coverage¶ (%)	LVA# (/× 10^3 μm^2)
Control	39.64 ± 5.24	6.94 ± 1.26	11.2 ± 1.48	6.90 ± 0.84	61.8 ± 9.89	81.50 ± 16.51
Nilotinib (100 mg/kg)	35.87 ± 1.75	6.82 ± 0.68	10.9 ± 0.82	4.34 ± 0.70**	31.8 ± 3.87**	7.21 ± 0.89††
Everolimus (2 mg/kg)	31.30 ± 4.54	13.8 ± 1.07††	6.5 ± 0.50**	1.66 ± 0.29††	57.8 ± 7.83	51.63 ± 10.23
Nilotinib (100 mg/kg) + everolimus (2 mg/kg)	13.15 ± 2.30††	11.0 ± 1.57**	7.2 ± 0.38	1.26 ± 0.14††	16.2 ± 4.98**	0.84 ± 0.37††

Ki-67 LI, Ki-67 labeling index; MVC, microvessel count; MVA, microvessel area; LVA, lymphatic vessel area.
Control mice were given water daily by oral gavage. Control group ($n = 5$), nilotinib group ($n = 5$), everolimus group ($n = 6$), and nilotinib and everlimus group ($n = 6$).
*Number (mean ± SE) of Ki-67–positive tumor cells per field determined by measuring 10 random 0.14-mm^2 fields at ×200 magnification.
†Percentage of TUNEL-positive tumor cells (out of total number of cells) per 0.14-mm^2 fields at ×200 magnification.
‡MVC was determined by counting 10 random fields at ×200 magnification.
§MVA was determined by measuring 10 random fields at ×200 magnification.
¶CD31-positive cells in direct contact with desmin-positive cells were counted in five random fields at ×200 magnification.
#LVA was determined by measuring 10 random fields at ×100 magnification.
**$P < .05$ *versus* control group values.
††$P < .01$ *versus* control group values.

Therefore, blockade of PDGF-R signaling by imatinib or nilotinib may decrease the stromal reaction, areas of lymphatic vessels, and number of pericytes. Inhibition of PDGF-Rβ phosphorylation in stromal cells was confirmed by immunofluorescence in the present study.

Everolimus is a rapalog, one of the mTOR inhibitors. The best characterized cellular effect of rapamycin on tumor cells is the growth retardation by cell cycle arrest in G_1 phase of the cell cycle [35]. Treatment with rapamycin at high concentrations results in an accumulation of cells in S phase and induction of apoptosis in certain cell systems [36]. Rapamycin is reported to reduce the production of VEGF by tumor cells and block VEGF-mediated stimulation of endothelial cells and tube formation [37]. Therefore, rapamycin administration can induce apoptosis of VEGF-stimulated endothelial cells, potentially leading to tumor vessel thrombosis [38]. These effects of rapamycin match our findings that treatment with everolimus induced apoptosis and inhibited VEGF expression of tumor cells.

The effects of rapamycin on lymphangiogenesis and lymph node metastasis were recently investigated in a nude mice model, and rapamycin significantly reduced the number and area of lymphatic vessels in the primary tumor [39,40]. Lymph node metastasis was significantly suppressed in the rapamycin-treated nude mice. The VEGF-C/vascular endothelial growth factor receptor-3 (VEGFR-3) signal transduction pathway plays a causal role in tumor-associated lymphangiogenesis and lymphatic metastasis [41]. Rapamycin repressed protein and mRNA expressions of VEGF-A and VEGF-C in B13LM cells under both serum-starved and normal culture conditions [40], suggesting that rapamycin inhibits lymphangiogenesis *in vivo* probably by inhibition of VEGF-C expression. Rapamycin also impairs downstream signaling of VEGF-A and VEGF-C through the mTOR/S6K1 pathway in lymphatic endothelial cells [39]. In our mouse model, inhibition of lymphangiogenesis was observed under treatment with nilotinib but not everolimus. Further studies are needed to determine whether everolimus inhibits lymphangiogenesis.

Rapalogs in combination with other anticancer agents, including standard chemotherapy agents, receptor tyrosine kinase–targeted agents, and angiogenesis inhibitors, have shown greater activity than single-agent rapalog, suggesting that rapalogs may be best used in combination therapies [42]. However, the mechanisms of increased efficacy have not been elucidated. The present study showed that PDGF-R inhibitor and rapalog inhibited activated stromal components and neoplastic cells, respectively. Combination therapy based on these drugs may block cancer-stromal interaction, and mTOR inhibitor appears promising as a therapeutic agent against stromal compartment–rich tumors.

Acknowledgments

The authors thank Shinichi Norimura for his excellent technical assistance. This work was carried out with the kind cooperation of the Analysis Center of Life Science and Institute of Laboratory Animal Science, Hiroshima University, and we thank Novartis Pharma KK for providing the imatinib, nilotinib, and everolimus.

References

[1] Jemal A, Bray F, Center MM, Ferlay J, Ward E, and Forman D (2011). Global cancer statistics. *CA Cancer J Clin* **61**, 69–90.

[2] Mantovani A, Allavena P, Sica A, and Balkwill F (2008). Cancer-related inflammation. *Nature* **454**, 436–444.

[3] Whiteside TL (2008). The tumor microenvironment and its role in promoting tumor growth. *Oncogene* **27**, 5904–5912.

[4] Mueller MM and Fusenig NE (2004). Friends or foes—bipolar effects of the tumour stroma in cancer. *Nat Rev Cancer* **4**, 839–849.

[5] Kitadai Y (2010). Cancer-stromal cell interaction and tumor angiogenesis in gastric cancer. *Cancer Microenviron* **3**, 109–116.

[6] Uehara H, Kim SJ, Karashima T, Shepherd DL, Fan D, Tsan R, Killion JJ, Logothetis C, Mathew P, and Fidler IJ (2003). Effects of blocking platelet-derived growth factor-receptor signaling in a mouse model of experimental prostate cancer bone metastases. *J Natl Cancer Inst* **95**, 458–470.

[7] Antoniades HN, Galanopoulos T, Neville-Golden J, and O'Hara CJ (1992). Malignant epithelial cells in primary human lung carcinomas coexpress *in vivo* platelet-derived growth factor (PDGF) and PDGF receptor mRNAs and their protein products. *Proc Natl Acad Sci USA* **89**, 3942–3946.

[8] Lindmark G, Sundberg C, Glimelius B, Påhlman L, Rubin K, and Gerdin B (1993). Stromal expression of platelet-derived growth factor beta-receptor and platelet-derived growth factor B-chain in colorectal cancer. *Lab Invest* **69**, 682–689.

[9] Seymour L, Dajee D, and Bezwoda WR (1993). Tissue platelet derived-growth factor (PDGF) predicts for shortened survival and treatment failure in advanced breast cancer. *Breast Cancer Res Treat* **26**, 247–252.

[10] Yi B, Williams PJ, Niewolna M, Wang Y, and Yoneda T (2002). Tumor-derived platelet-derived growth factor-BB plays a critical role in osteosclerotic bone metastasis in an animal model of human breast cancer. *Cancer Res* **62**, 917–923.

[11] Sumida T, Kitadai Y, Shinagawa K, Tanaka M, Kodama M, Ohnishi M, Ohara E, Tanaka S, Yasui W, and Chayama K (2011). Anti-stromal therapy with imatinib inhibits growth and metastasis of gastric carcinoma in an orthotopic nude mouse model. *Int J Cancer* **128**, 2050–2062.

[12] Kodama M, Kitadai Y, Sumida T, Ohnishi M, Ohara E, Tanaka M, Shinagawa K, Tanaka S, Yasui W, and Chayama K (2010). Expression of platelet-derived growth factor (PDGF)-B and PDGF-receptor β is associated with lymphatic metastasis in human gastric carcinoma. *Cancer Sci* **101**, 1984–1989.

[13] Ostman A (2004). PDGF receptors-mediators of autocrine tumor growth and regulators of tumor vasculature and stroma. *Cytokine Growth Factor Rev* **15**, 275–286.

[14] Risau W, Drexler H, Mironov V, Smits A, Siegbahn A, Funa K, and Heldin CH (1992). Platelet-derived growth factor is angiogenic *in vivo*. *Growth Factors* **7**, 261–266.

[15] Bergers G, Song S, Meyer-Morse N, Bergsland E, and Hanahan D (2003). Benefits of targeting both pericytes and endothelial cells in the tumor vasculature with kinase inhibitors. *J Clin Invest* **111**, 1287–1295.

[16] Pietras K (2004). Increasing tumor uptake of anticancer drugs with imatinib. *Semin Oncol* **31**, 18–23.

[17] Druker BJ and Lydon NB (2000). Lessons learned from the development of an abl tyrosine kinase inhibitor for chronic myelogenous leukemia. *J Clin Invest* **105**, 3–7.

[18] Fletcher JA (2004). Role of KIT and platelet-derived growth factor receptors as oncoproteins. *Semin Oncol* **31**, 4–11.

[19] Day E, Waters B, Spiegel K, Alnadaf T, Manley PW, Buchdunger E, Walker C, and Jarai G (2008). Inhibition of collagen-induced discoidin domain receptor 1 and 2 activation by imatinib, nilotinib and dasatinib. *Eur J Pharmacol* **599**, 44–53.

[20] Weisberg E, Manley PW, Breitenstein W, Brüggen J, Cowan-Jacob SW, Ray A, Huntly B, Fabbro D, Fendrich G, Hall-Meyers E, et al. (2005). Characterization of AMN107, a selective inhibitor of native and mutant Bcr-Abl. *Cancer Cell* **7**, 129–141.

[21] Manley PW, Stiefl N, Cowan-Jacob SW, Kaufman S, Mestan J, Wartmann M, Wiesmann M, Woodman R, and Gallagher N (2010). Structural resemblances and comparisons of the relative pharmacological properties of imatinib and nilotinib. *Bioorg Med Chem* **18**, 6977–6986.

[22] Corso G, Velho S, Paredes J, Pedrazzani C, Martins D, Milanezi F, Pascale V, Vindigni C, Pinheiro H, Leite M, et al. (2011). Oncogenic mutations in gastric cancer with microsatellite instability. *Eur J Cancer* **47**, 443–451.

[23] Wen YG, Wang Q, Zhou CZ, Qiu GQ, Peng ZH, and Tang HM (2010). Mutation analysis of tumor suppressor gene *PTEN* in patients with gastric carcinomas and its impact on PI3K/AKT pathway. *Oncol Rep* **24**, 89–95.

[24] Murayama T, Inokuchi M, Takagi Y, Yamada H, Kojima K, Kumagai J, Kawano T, and Sugihara K (2009). Relation between outcomes and localisation of p_mTOR expression in gastric cancer. *Br J Cancer* **100**, 782–788.

[25] An JY, Kim KM, Choi MG, Noh JH, Sohn TS, Bae JM, and Kim S (2010). Prognostic role of p-mTOR expression in cancer tissues and metastatic lymph nodes in pT2b gastric cancer. *Int J Cancer* **126**, 2904–2913.

[26] Falcon BL, Barr S, Gokhale PC, Chou J, Fogarty J, Depeille P, Miglarese M, Epstein DM, and McDonald DM (2011). Reduced VEGF production, angiogenesis, and vascular regrowth contribute to the antitumor properties of dual mTORC1/mTORC2 inhibitors. *Cancer Research* **71**, 1573–1583.

[27] Guertin DA and Sabatini DM (2007). Defining the role of mTOR in cancer. *Cancer Cell* **12**, 9–22.

[28] Agarwal NK, Chen CH, Cho H, Boulbès DR, Spooner E, and Sarbassov DD (2013). Rictor regulates cell migration by suppressing RhoGDI2. *Oncogene* **32**, 2521–2526.

[29] Wan X, Mendoza A, Khanna C, and Helman LJ (2005). Rapamycin inhibits ezrin-mediated metastatic behavior in a murine model of osteosarcoma. *Cancer Res* **65**, 2406–2411.

[30] Apte SM, Fan D, Killion JJ, and Fidler IJ (2004). Targeting the platelet-derived growth factor receptor in antivascular therapy for human ovarian carcinoma. *Clin Cancer Res* **10**, 897–908.

[31] Kobie K, Kawabata M, Hioki K, Tanaka A, Matsuda H, Mori T, and Maruo K (2007). The tyrosine kinase inhibitor imatinib [STI571] induces regression of xenografted canine mast cell tumors in SCID mice. *Res Vet Sci* **82**, 239–241.

[32] Wolff NC, Veach DR, Tong WP, Bornmann WG, Clarkson B, and Ilaria RL Jr (2005). PD166326, a novel tyrosine kinase inhibitor, has greater antileukemic activity than imatinib mesylate in a murine model of chronic myeloid leukemia. *Blood* **105**, 3995–4003.

[33] Yokoi K, Sasaki T, Bucana CD, Fan D, Baker CH, Kitadai Y, Kuwai T, Abbruzzese JL, and Fidler IJ (2005). Simultaneous inhibition of EGFR, VEGFR, and platelet-derived growth factor receptor signaling combined with gemcitabine produces therapy of human pancreatic carcinoma and prolongs survival in an orthotopic nude mouse model. *Cancer Res* **65**, 10371–10380.

[34] Valiathan RR, Marco M, Leitinger B, Kleer CG, and Fridman R (2012). Discoidin domain receptor tyrosine kinases: new players in cancer progression. *Cancer Metastasis Rev* **31**, 295–321.

[35] Albanell J, Dalmases A, Rovira A, and Rojo F (2007). mTOR signalling in human cancer. *Clin Transl Oncol* **9**, 484–493.

[36] Saunders PO, Weiss J, Welschinger R, Baraz R, Bradstock KF, and Bendall LJ (2013). RAD001 (everolimus) induces dose-dependent changes to cell cycle regulation and modifies the cell cycle response to vincristine. *Oncogene* **32**, 4789–4797.

[37] Guba M, von Breitenbuch P, Steinbauer M, Koehl G, Flegel S, Hornung M, Bruns CJ, Zuelke C, Farkas S, Anthuber M, et al. (2002). Rapamycin inhibits primary and metastatic tumor growth by antiangiogenesis: involvement of vascular endothelial growth factor. *Nat Med* **8**, 128–135.

[38] Bruns CJ, Koehl GE, Guba M, Yezhelyev M, Steinbauer M, Seeliger H, Schwend A, Hoehn A, Jauch KW, and Geissler EK (2004). Rapamycin-induced endothelial cell death and tumor vessel thrombosis potentiate cytotoxic therapy against pancreatic cancer. *Clin Cancer Res* **10**, 2109–2119.

[39] Huber S, Bruns CJ, Schmid G, Hermann PC, Conrad C, Niess H, Huss R, Graeb C, Jauch KW, Heeschen C, et al. (2007). Inhibition of the mammalian target of rapamycin impedes lymphangiogenesis. *Kidney Int* **71**, 771–777.

[40] Kobayashi S, Kishimoto T, Kamata S, Otsuka M, Miyazaki M, and Ishikura H (2007). Rapamycin, a specific inhibitor of the mammalian target of rapamycin, suppresses lymphangiogenesis and lymphatic metastasis. *Cancer Sci* **98**, 726–733.

[41] He Y, Kozaki K, Karpanen T, Koshikawa K, Yla-Herttuala S, Takahashi T, and Alitalo K (2002). Suppression of tumor lymphangiogenesis and lymph node metastasis by blocking vascular endothelial growth factor receptor 3 signaling. *J Natl Cancer Inst* **94**, 819–825.

[42] Zhou HY and Huang SL (2012). Current development of the second generation of mTOR inhibitors as anticancer agents. *Chin J Cancer* **31**, 8–18.

European Journal of Radiology 82 (2013) 169–176

Contents lists available at SciVerse ScienceDirect

European Journal of Radiology

journal homepage: www.elsevier.com/locate/ejrad

Evaluation of the efficacy of the guideline on reading CT images of malignant pleural mesothelioma with reference CT films for improving the proficiency of radiologists

Huashi Zhou[a,1], Taro Tamura[a,2], Yukinori Kusaka[a,*], Narufumi Suganuma[b,3], Ponglada Subhannachart[c,4], Chomphunut Vijitsanguan[c,4], Weeraya Noisiri[c,4], Kurt G. Hering[d,5], Masanori Akira[e,6], Harumi Itoh[a,f,7], Hiroaki Arakawa[g,8], Yuichi Ishikawa[h,9], Shinji Kumagai[i,10], Norio Kurumatani[j,11]

[a] Department of Environmental Health, School of Medicine University of Fukui, 23-3 Shimoaitsuki, Matsuoka, Eihezi-cho, Fukui Prefecture, 910-1193, Japan
[b] Department of Environmental Medicine, Kochi University School of Medicine, Japan
[c] Central Chest Disease Institute of Thailand, 39 Moo 9, Tiwanon Road, Muang Nonthaburi, 11000, Thailand
[d] Department of Diagnostic Radiology, Radiooncology and Nuclear Medicine, Radiological Clinic, Miner's Hospital, Radiologische Klinik, Lansppaschaftskranhaus Dortmund, Wieckesweg 27, 44309, Dortmund, Germany
[e] Department of Radiology, National Hospital Organization Kinki-Chuo Chest Medical Center, 1180 Nagasone-cho, Kita-ku, Sakai, Osaka, 591-8555, Japan
[f] Department of Radiology, School of Medicine, University of Fukui, 23-3 Shimoaitsuki Matsuoka, Eiheizi-cho, Fukui Prefecture, 910-1193, Japan
[g] Department of Radiology, Dokkyo University School of Medicine, 880 Oaza-Kitakobayashi, Mibu-cho, Shimotsuga-gun, Tochigi, 321-0207, Japan
[h] Department of Pathology, Cancer Institute, 1-37-1 Kami-ikebukuro, Toshima-ku, Tokyo, 170-8455, Japan
[i] Department of Environmental Management, School of Health Sciences, University of Occupational and Environmental Health, University of Occupational and Environmental Health, 1-1, Iseigaoka, Yahata-nishi-ku, Fukuoka, Kitakyushu, 807-8555, Japan
[j] Department of Community Health and Epidemiology, Nara Medical University School of Medicine, 840 Shijo-cho Kashihara, Nara, 634-8521, Japan

ARTICLE INFO

Article history:
Received 2 March 2012
Received in revised form 20 May 2012
Accepted 21 May 2012

Keywords:
Computed tomography
Malignant pleural mesothelioma
Guideline
Sensitivity
Specificity
Agreement

ABSTRACT

Purpose: To assess the efficacy of the developed guideline on reading CT images of malignant pleural mesothelioma for improving radiologists' reading proficiency.
Materials and Methods: Three radiologists independently read the CT films of 22 cases including definite mesothelioma and non-mesothelioma cases at two times before and after studying the malignant pleural mesothelioma CT Guideline. The sensitivity and specificity for mesothelioma were calculated and compared between the 1st and 2nd trials. The kappa statistics was examined for agreement with experts for mesothelioma probability and for mesothelioma features recorded by three radiologists.
Results: After studying the mesothelioma CT Guideline, the sensitivity for mesothelioma shown by the three radiologists at the 2nd trial was 100%, 100% and 80%, which were higher than 80%, 85% and 60% at the 1st trial, respectively. The average kappa for agreement between radiologists and experts on dichotomized mesothelioma probability were 0.69 (good) at the 2nd trial vs. 0.38 (fair) at the 1st trial. The average kappa for the agreement with experts for each of 7 features by three radiologists were 0.52–0.80 at the 2nd trial, which were significantly higher than 0.34–0.58 at the 1st trial (Wilcoxon Signed Rank Test: $P<0.01$), and as to five features "unilateral pleural effusion", "nodular pleural thickening", "tumoral encasement of lung", "mediastinal pleural thickening", and "diminished lung", they achieved good agreement with average kappa of 0.61–0.80.
Conclusion: The developed mesothelioma CT Guideline was suggested to have substantial effect in improving the radiologists' proficiency for reading CT images of mesothelioma, and may contribute to accurate diagnosis of mesothelioma.

* Corresponding author. Tel.: +81 776 61 8335; fax: +81 776 61 8107.
E-mail addresses: zhouhua@u-fukui.ac.jp (H. Zhou), tarou@u-fukui.ac.jp (T. Tamura), kusakayk@gmail.com (Y. Kusaka), nsuganuma@kochi-u.ac.jp (N. Suganuma), pongladas@gmail.com (P. Subhannachart), Chompoo_vj@yahoo.com (C. Vijitsanguan), weeraya_tat@yahoo.com (W. Noisiri), k.g.hering@t-online.de (K.G. Hering), akira@kch.hosp.go.jp (M. Akira), hitoh@fmsrsa.fukui-med.ac.jp (H. Itoh), arakawa@dokkyomed.ac.jp (H. Arakawa), ishikawa@jfcr.or.jp (Y. Ishikawa), shkumagai@health.uoeh-u.ac.jp (S. Kumagai), knorio@naramed-u.ac.jp (N. Kurumatani).
[1] Tel.: +81 776 61 8338; fax: +81 776 61 8107.
[2] Tel.: +81 776 61 8335; fax: +81 776 61 8107.
[3] Tel.: +81 88 880 2407; fax: +81 88 880 2407.
[4] Tel.: +66 2 5803423x7505; fax: +66 2 5806992.
[5] Tel.: +49 0 231 9221280; fax: +49 0 231 9221648.
[6] Tel.: +81 722 52 3021; fax: +81 722 51 1372.
[7] Tel.: +81 776 61 8368; fax: +81 776 61 8137.
[8] Tel.: +81 282 87 2171; fax: +81 282 86 4940.
[9] Tel.: +81 3 3570 0448; fax: +81 3 3570 0558.
[10] Tel.: +81 93 691 7282; fax: +81 93 691 2694.
[11] Tel.: +81 744 298841; fax: +81 744 290673.

0720-048X/$ – see front matter © 2012 Elsevier Ireland Ltd. All rights reserved.
http://dx.doi.org/10.1016/j.ejrad.2012.05.022

1. Introduction

The *International Classification of HRCT for Occupational and Environmental Respiratory Diseases* (ICOERD) was developed and used for occupational diseases screening, epidemiology study, and clinical study for respiratory diseases caused by occupational and environmental factors [1]. In order to supply ICOERD, we have developed the *Guideline on Reading CT Films of Malignant Pleural Mesothelioma* (MPM-CT Guideline) and selected MPM reference CT films [2]. The MPM-CT Guideline provides the terminology of MPM CT features and the MPM probability, the judgment for MPM in terms of involvement distribution and severity, as well as a method to record the CT finding of MPM on the CT reading sheet. The purpose of the current study was to investigate the efficacy of the developed MPM-CT Guideline with the MPM reference CT films for improving the proficiency of the inexperienced radiologists in reading CT images of MPM.

2. Materials and methods

2.1. Subject CT films

CT films of fifty seven cases including MPM, lung cancer, other malignancies, and benign pleural plaque were collected from the citizens living in the neighborhood of the Kubota factory, a large asbestos cement pipe factory in Amagasaki City, Hyogo Prefecture, Japan. Their MPM was caused by environmental exposure to asbestos (mainly crocidolite) air pollution from the Kubota asbestos factory [3].

Out of the 57 cases, 22 cases including 20 definite MPM cases and 2 pleural plaque cases were subjected to study. The MPM cases were clinically diagnosed as MPM at local hospitals and both pathologically and immunohistochemically confirmed [4,5]. Among the 20 cases of MPM, 7 cases were female, and 13 cases were male. The two cases of pleural plaque were male.

Among the 20 MPM cases, the diffuse type of MPM accounted for 18 (90%), and the localized type for the other 2 cases (10%). The numbers of the cases with MPM CT features among 20 MPM cases by MPM probability are shown in Table 1. The CT images of several representative MPM cases among the 20 MPM cases are shown as Figs. 1–5.

2.2. The MPM reference CT films

The MPM reference CT films and CT subject images were used by radiologists only at the 2nd reading trial for comparison of the subjects' CT findings with MPM reference films. The ten typical MPM features on the reference CT films included "unilateral pleural effusion" ("ue"), "nodular pleural thickening" ("nt"), "interlobar fissure thickening" ("it"), "mediastinal pleural thickening" ("mt"), "tumoral encasement of lung" ("te"), "calcified plaque engulfment" ("pe"), "invasion" (iv"), "diminished lung" ("dl"), "contracted hemithorax" ("ch") and "pleural mass" ("pm"). Each MPM feature was indicated by an arrow on the reference CT digital images and hard-copied CT reference films. The CT images of typical MPM features are shown as in Fig. 1 through Fig. 9 in a parallel publication [2].

2.3. CT reading trials of 22 cases by three radiologists

Three radiologists participated in independent reading of CT films. All of the radiologists had good proficiency and rich experience in reading CT for pneumoconioses. However, they had not seen many MPM cases previously. Before achieving the 1st and 2nd reading trials, they were blinded to the information of the patients' asbestos exposure history, and the clinical and histological diagnosis for any cases.

At the 1st CT reading trial, the three radiologists were requested to read the monograph of ICOERD and the ICOERD CT reference films, but not to read the MPM-CT Guideline nor the MPM reference CT films, then they read the 22 subject CT films independently. The CT findings associated with asbestosis were recorded according to ICOERD guideline; the MPM features and the MPM probability grade for each case were recorded into the reading sheet according to their experiences.

The interval between the 1st and the 2nd CT reading trials by the three radiologists was at least three months. At the 2nd trial, before reading the subject CT films, the three radiologists read the ICOERD guideline with the ICOERD CT reference films again. They also independently studied the MPM-CT Guideline with the MPM reference CT films, and then independently read the 22 subject CT films. They made use of the ICOERD CT reference films and the MPM reference CT films to record the CT findings for pneumoconiosis, the MPM findings, and the MPM probability grade in the CT reading sheets.

2.4. Statistical analysis

According to the definition for the MPM probability in the MPM-CT Guideline [2], Grade 1 was negative for MPM, no abnormal findings on CT, or the abnormal findings of other diseases; Grade 2 was low probability of MPM; Grade 3 was moderate probability of MPM; Grade 4 was high probability of MPM. Sensitivity for MPM was the proportion of cases for which MPM probability Grade ≥ 2 recorded by radiologists for each among the 20 MPM cases. Specificity for MPM was the proportion of cases for which MPM probability Grade = 1 was recorded by individual radiologists among the 2 non-MPM cases, shown as Table A in Supplementary Appendix. The sensitivity and specificity for MPM by the three radiologists were calculated and compared between the 1st and the 2nd reading trials.

The weighted kappa for the agreement of the three individual radiologists with the consensus by the four experts (K.G.H., M.A., H. A., H. I.) on the 4-point scale MPM probability was calculated using R-software version 2.14.1 (http://www.r-project.org/), as shown in Table B in Supplementary Appendix. The kappa for the agreement on dichotomized MPM probability was calculated by stratifying the cases with MPM probability Grade 2, 3, 4 into one group, and the cases with MPM probability Grade = 1 into the other group, as shown in Table C in the Supplementary Appendix. The observed agreement on dichotomized MPM probability between radiologist and experts was also calculated. The calculation of kappa for the agreement on MPM CT feature between radiologist and experts is shown as Table D in the Supplementary Appendix. A kappa value <0.20 was considered as poor agreement, 0.21–0.40 was as fair agreement, 0.41–0.60 was as moderate agreement, 0.61–0.80 was as good agreement, and 0.81–1.00 was as excellent agreement [6]. The kappa values for the 7 MPM CT features by the three radiologists between the 1st trial and 2nd trial were compared by 2-Related-Samples Nonparametric Test (Wilcoxon Signed Rank Test).

3. Results

3.1. The MPM probability and the 7 MPM CT features among the 20 MPM cases

The MPM probability and the 7 MPM CT features (7-MPM-CT features) agreed by the four experienced experts for the 20 subject cases of MPM are shown as Table 1.

Table 1
The number of cases with the 7-MPM-CT features among the 20 MPM cases according to MPM probability.

Cases with MPM probability	The number of cases with the MPM feature						
	ue	nt	it	mt	te	iv	dl
Grade = 1 (n = 0)	0	0	0	0	0	0	0
Grade = 2 (n = 3)	0	1	0	0	0	2	0
Grade = 3 (n = 7)	5	2	4	7	0	1	4
Grade = 4 (n = 10)	8	10	7	10	5	6	10
Total (n = 20)	13(65%)	13(65%)	11(55%)	17(85%)	5(25%)	9(45%)	14(70%)

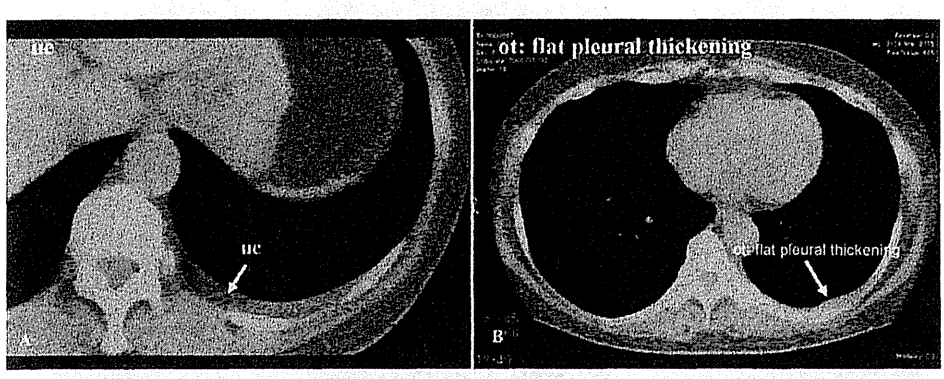

Fig. 1. A 52-year-old women with diffuse epithelioid MPM. CT scans show slight unilateral pleural effusion (A) and flat pleural thickening in the left hemithorax (B). According to the CT appearance, the MPM probability was agreed as low probability Grade 2 at mild severity by experts.

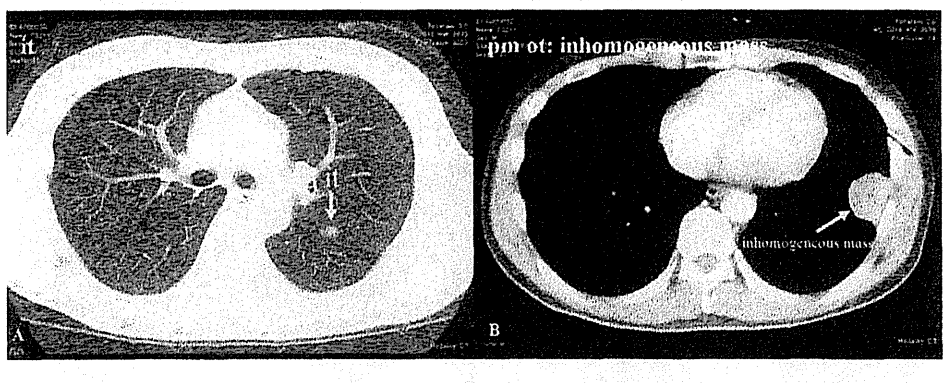

Fig. 2. A 49-year-old man with biphasic MPM. CT scans show interlobar fissure pleural thickening ("it") at the left lung (A), and the left-side pleural mass with involvement of chest wall (B). According the CT appearance, the MPM probability was agreed by experts as low probability Grade 2. The differential diagnosis for this case is mainly sarcoma.

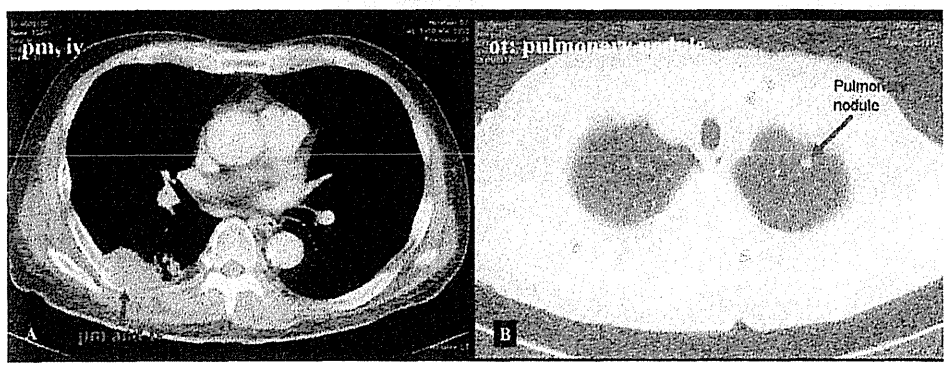

Fig. 3. A 68-year-old man with localized sarcomatoid MPM. CT scan demonstrates a right-sided pleural mass invasion ("iv") to the chest wall destroying rib structure (arrow) (A). There is a pulmonary nodule on the left lung (B). This case was agreed as MPM of moderate probability Grade 3 at advanced severity. The different diagnosis is firstly sarcoma and secondly possible metastasis from other cancer.

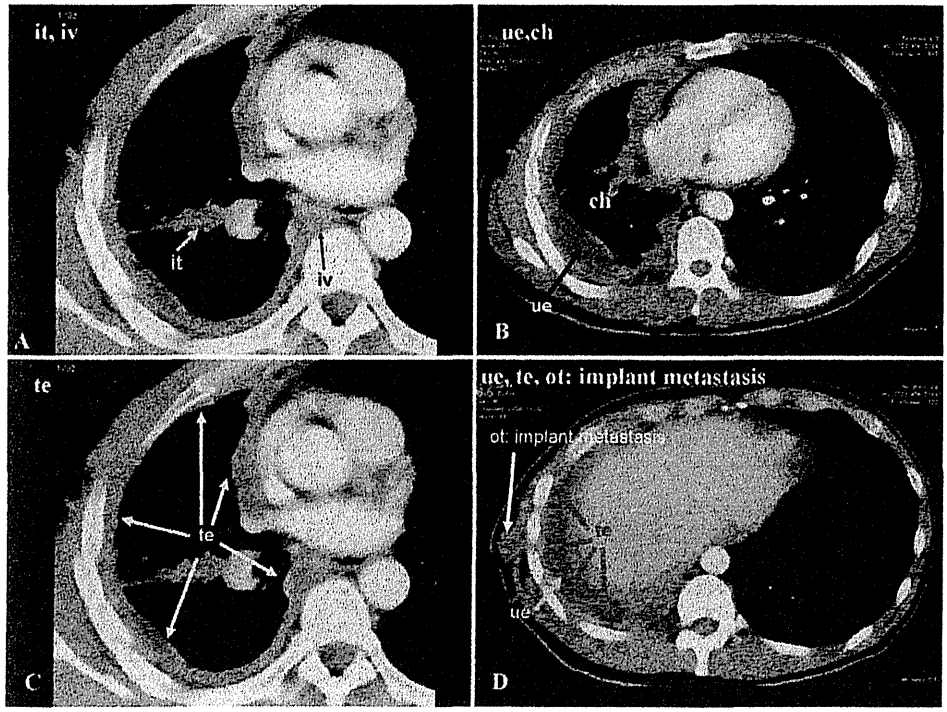

Fig. 4. A 45-year-old man with diffuse epithelioid MPM. CT scan shows interlobar fissure pleural thickening (A), invasion to the tissue near to the vertebral column ("iv") (black arrow) (A). There is unilateral pleural effusion ("ue") (black arrow) on the right hemithorax, leading to the contracted hemithorax ("ch") (B). Tumoral encasement of lung ("te") involvement on the right hemithorax (C, D) and an implant metastasis lesion are observed on the chest wall of right lung (D). According the CT appearance, MPM probability was agreed by experts as high probability Grade 4 at advanced severity. This is a typical MPM case.

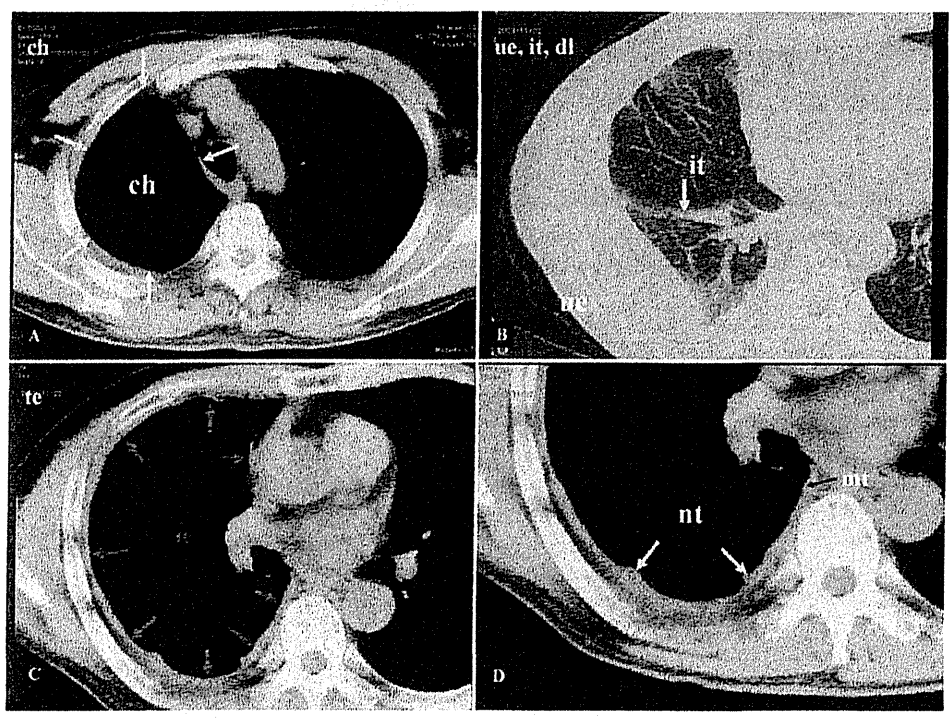

Fig. 5. A 58 year-old man with diffuse desmoplastic MPM. CT scan shows contracted hemithorax ("ch") leading to the right hemithorax volume loss (A). There is interlobar fissure pleural thickening ("it"), together with unilateral pleural thickening ("ue"), causing the lung volume diminished ("dl") (B). The involvement of tumoral encasement of lung ("te") (C), nodular pleural thickening ("nt") and mediastinal pleural thickening ("mt") (black arrow) on the right hemithorax are observed (D). MPM probability was agreed by experts as high MPM probability Grade 4 at advanced severity. This is a typical MPM case.

Table 2
Agreement on dichotomized MPM probability with 4 experts' consensus and sensitivity and specificity for MPM by three radiologists at the two trials.

Reader	Reading trial	Agreement with experts on dichotomized MPM probability	Sensitivity for MPM	Specificity for MPM
Radiologist 1	1st	18/22(81.82%)	16/20(80%)	2/2(100%)
	2nd	21/22(95.45%)	20/20(100%)	1/2(50%)
Radiologist 2	1st	19/22(86.36%)	17/20(85%)	2/2(100%)
	2nd	22/22(100%)	20/20(100%)	2/2(100%)
Radiologist 3	1st	14/22(63.64%)	12/20(60%)	2/2(100%)
	2nd	18/22(81.82%)	16/20(80%)	2/2(100%)

Among the 20 definite MPM cases, the cases with MPM probability Grade 2, Grade 3 and Grade 4 accounted for 3/20 (15%), 7/20 (35%) and 10/20 (50%), respectively.

For the 3 cases with MPM probability Grade 2, the cases with the feature "nodular pleural thickening" ("nt") accounted for 1/3(33.33%), and the cases with "invasion" ("iv") accounted for 2/3 (66.67%).

Among the 7 cases with MPM probability Grade 3, the cases with feature "medialstinal pleural thickening" ("mt") accounted for 7/7 (100%), the feature of "unilateral pleural effusion" ("ue") were present in 5/7 (71.43%), "interlobar fissure thickening" ("it") in 4/7 (57.14%), "diminished lung" ("dl") in 4/7 (57.14%), "nt" in 2/7 (28.57%), and "iv" in 1/7 (14.29%).

Among the 10 cases with MPM probability Grade 4, the most frequently recorded features were "nt" in 10/10 (100%), "mt" in 100%, and "dl" in 100%. The cases with feature "ue" were in 80%, "it" in 70%, "iv" in 60%, and "tumoral encasement of lung" in 50%.

3.2. The sensitivity and specificity for MPM by three radiologists, the agreement on MPM probability by radiologists with experts

The sensitivity for MPM, specificity for MPM and observed agreement on the dichotomized MPM probability by 3 radiologists at two times of CT readings before and after studying the MPM-CT Guideline are shown as in Table 2.

The sensitivity for MPM by the three radiologists at the 2nd trial was 100%, 100% and 80%, which was higher than 80%, 85% and 60%, respectively at the 1st reading trial. The observed agreements on dichotomized MPM probability by radiologists were increased at the 2nd trial compared with those at the 1st trial.

The values of weighted kappa for the agreement of MPM probability on the 4-point scale by three radiologists with experts were increased at the 2nd trial, compared with those at the 1st trial, as shown in Table 3.

The weighted kappa values for the agreement with experts on 4-point scale MPM probability by three radiologists were 0.32, 0.51 and 0.37 at the 2nd trial vs 0.24, 0.48 and 0.29 at the 1st trial, respectively. The kappa value for inter-reader agreements on the dichotomized MPM probability between radiologists and experts at the 2nd reading trial were 0.65 (good), 1 (excellent) and 0.42 (moderate), respectively, which were significantly higher than 0.42 (moderate), 0.51 (moderate) and 0.21 (fair) at the 1st trial, respectively. The average kappa for the agreement on dichotomized MPM probability between radiologists and experts were 0.69 (good) at the 2nd trial vs 0.38 (fair) at the 1st trial, which seemed to show an upgrading in reading skill.

3.3. The agreement on MPM features between radiologists and experts

The results of the agreements for the recorded MPM features between the three radiologists and experts are shown as in Table 4.

For radiologist 1, the agreement with experts for 6 features "unilateral pleural effusion" ("ue"), "nodular pleural thickening" ("nt"), "interlobar fissure thickening"("it"), "mediastinal pleural thickening" ("mt"), "invasion" ("iv") and "diminished lung" ("dl") at the 2nd reading trial was better compared with those at the 1st trial. The agreement for feature "ue" and "nt" at the 2nd trial was good (kappa = 0.62 and 0.61, respectively). The agreement for feature "tumoral encasement of lung" ("te") at the 2nd trial was excellent to the same extent as that at the 1st trial (kappa = 0.86). The agreement with experts on 3 features ("mt", "iv" and "dl") was markedly increased to excellent (kappa > 0.8) at the 2nd trial.

For radiologist 2, the kappa values for the agreement with experts were increased for 5 features ("ue", "nt", "mt", "te" and "dl") at the 2nd trial in comparison with those at the 1st trial. The kappa values for the features "ue", "nt" and "te" showed good agreement with experts (kappa > 0.6), and "mt" and "dl" showed excellent agreement (kappa > 0.8). The kappa values for the feature "it" and "iv" was 0.55 and 0.51 at the 2nd trial, which were lower than 0.73 and 0.61 at the 1st trial, respectively.

For the radiologist 3, the kappa values for 5 features ("nt", "mt", "te", "iv" and "dl") were increased at the 2nd trial in comparison with the 1st trial. The feature "nt" and "te" shows good agreement with expert (kappa = 0.64 and 0.77, respectively). The kappa value for the feature "it" at the 2nd trial was equal to that one at the 1st trial. The kappa value for the feature "ue" (0.49) at the 2nd trial was lower than at the 1st trial (0.65).

The average kappa values of 7 MPM CT features at the 2nd trial by the three radiologists were significantly increased in comparison with the 1st trial, and the six features "ue", "nt", "mt", "te" and "dl" showed good agreement between radiologists and experts (kappa > 0.60).

Table 5 shows that the kappa values for the agreement on the 7 MPM CT features by the three radiologists with experts were significantly higher than those at the 1st trial.

Table 3
Agreement on 4-point scale MPM probability and dichotomized MPM probability between radiologist and experts in terms of weighted kappa.

Reader	4-scale MPM probability K_w (95% CI)		Dichotomized MPM probability K_w (95% CI)	
	1st trial	2nd trial	1st trial	2nd trial
Radiologist 1	0.24 (−0.06, 0.54)	0.32 (0.06, 0.58)	0.42 (−0.09, 0.93)	0.65 (−0.03, 1)
Radiologist 2	0.48 (0.19, 0.76)	0.51 (0.24, 0.78)	0.51 (−0.01, 1)	1
Radiologist 3	0.29 (0.04, 0.53)	0.37 (0.12, 0.62)	0.21 (−0.22, 0.65)	0.42 (−0.09, 0.93)
Weighted kappa Mean(SD)	0.34 (0.13)	0.40 (0.10)	0.38(0.15)	0.69(0.29)